Synergistic and toxicity-reducing effects of acteoside as an adjuvant therapy of oxaliplatin against hepatocellular carcinoma

LIMEI WEN[1-3], JIAWEI ZHANG[4], BOWEI JU[2,4], ZHENG RAN[5], HAIBO ZHANG[1,2], YUCHENG LIAO[6], LIN CAO[7], QIANG HOU[7], JUNPING HU[7] and JIANHUA YANG[1,2]

[1]Department of Pharmacy, The First Affiliated Hospital of Xinjiang Medical University, Urumqi, Xinjiang 830011, P.R. China; [2]Xinjiang Key Laboratory of Clinical Drug Research, The First Affiliated Hospital of Xinjiang Medical University, Urumqi, Xinjiang 830011, P.R. China; [3]State Key Laboratory of Neurology and Oncology Drug Development, Simcere Pharmaceutical Group Co., Ltd, Nanjing, Jiangsu 210042, P.R. China; [4]Department of Pharmacy, The Fifth Affiliated Hospital of Xinjiang Medical University, Urumqi, Xinjiang 830011, P.R. China; [5]Department of Pharmacy, The First Affiliated Hospital of Chongqing Medical University, Chongqing 400016, P.R. China; [6]Department of Pharmacy, Xijing Hospital, Fourth Military Medical University, Xi'an, Shaanxi 710032, P.R. China; [7]College of Pharmacy, Xinjiang Medical University, Urumqi, Xinjiang 830054, P.R. China

Received October 8, 2024; Accepted April 4, 2025

DOI: 10.3892/ijo.2025.5751

Abstract. Oxaliplatin (OXA) is a first-line chemotherapy agent for hepatocellular carcinoma (HCC); however, its application is hindered by low therapeutic sensitivity and severe adverse effects. Acteoside (ACT) has both antitumor and hepatoprotective properties. Therefore, the present study investigated the mechanisms underlying the synergistic and toxicity-reducing effects of ACT as an adjuvant to OXA in HCC therapy. Liver cancer cell lines and a xenograft mouse model were treated with ACT and/or OXA. *In vitro* Cell Counting kit-8, Transwell invasive assay, wound healing assay, cell cycle and apoptosis detection assays assessed cell viability, migration, invasion, cell cycle progression and apoptosis to evaluate the synergistic effects of the combination therapy. *In vivo* studies examined tumor growth, cell proliferation, survival time and blood biochemical indices. The effects of ACT on OXA-induced toxicity were also evaluated. Transcriptomics and metabolomics analyses were integrated to elucidate the mechanisms by which ACT enhances OXA efficacy and mitigates its toxicities. The results revealed that ACT synergized with OXA to inhibit HCC progression both *in vivo* and *in vitro*. ACT significantly alleviated OXA-induced toxicity, particularly neurotoxicity. Mechanistically, phosphatidylinositol signaling system-associated genes/proteins exerted important roles in the anti-HCC effects of ACT. Western blotting revealed that ACT-induced upregulation of INPP4B inhibited the PI3K/AKT signaling pathway, which may underlie its ability to enhance the therapeutic efficacy of OXA and reduce its toxic effects. In conclusion, ACT enhanced efficacy and reduced the toxicity of OXA in the treatment of HCC, potentially via the regulation of INPP4B to inhibit the PI3K/AKT signaling pathway.

Correspondence to: Dr Jianhua Yang, Department of Pharmacy, The First Affiliated Hospital of Xinjiang Medical University, 137 Liyushan South Road, Urumqi, Xinjiang 830011, P.R. China
E-mail: yjh_yfy@163.com

Dr Junping Hu, College of Pharmacy, Xinjiang Medical University, 393 Xinyi Road, Urumqi, Xinjiang 830054, P.R. China
E-mail: hjp_yxy@163.com

Key words: hepatocellular carcinoma, acteoside, oxaliplatin, synergistic effect, OXA-induced toxicity, mechanism

Introduction

Hepatocellular carcinoma (HCC) is the fifth most common malignancy and the second leading cause of cancer-associated mortality worldwide (1). Despite notable advancements, HCC remains a global public health challenge due to its poor prognosis and limited treatment options (2). The oxaliplatin (OXA)-based FOLFOX4 regimen, combining OXA with 5-fluorouracil and leucovorin, is one of the approved by National Comprehensive Cancer Network as first-line therapies for HCC (3,4). However, its clinical efficacy is hindered by drug resistance, decreased chemosensitivity (5) and severe side effects (6,7), including dose-dependent OXA-induced neurotoxicity (OXIN), which affects 85-95% of patients (8). Furthermore, compared with other malignancies, HCC has lower sensitivity to OXA, leading to suboptimal therapeutic outcomes (9).

To address these limitations, recent studies have increasingly focused on combination strategies that enhance treatment efficacy while mitigating toxicity (10-12). The 'synergistic and toxicity-reducing' approach, which aims to boost therapeutic outcomes while decreasing chemotherapy-induced adverse effects, has shown promise in improving long-term survival for patients with cancer (13). However, while studies on synergistic effects are relatively abundant, research on toxicity reduction remains limited (14-16).

Chinese medicinal herbs, known for broad bioactive properties, high safety profiles and minimal side effects

during long-term use, have emerged as valuable candidates for adjuvant therapy in cancer treatment (17). Herba Cistanches, a medicinal herb native to Xinjiang, China, has demonstrated diverse pharmacological effects, such as liver protection, anti-oxidation and anti-inflammatory properties (18-20). In our previous study, Herba Cistanches was shown to alleviate OXIN and improve the quality of life of patients undergoing OXA-based chemotherapy for gastrointestinal tumors (21). Moreover, phenylethanol glycosides from Herba Cistanches have been reported to enhance the therapeutic effects of OXA on hepatic cancer (22).

Acteoside (ACT), a phenylethanoid glycoside extracted from Herba Cistanche, has received increased attention due to its antitumor, anti-oxidative, immunomodulatory and anti-inflammatory properties (23-25). It has shown anticancer effects in cancer cell lines by regulating multiple cancer-associated signaling pathways in diverse preclinical and non-preclinical models (26,27). Notably, ACT has been reported to modulate oxidative stress and apoptosis in hepatic cancer (28,29), and to antagonize hepatitis B virus (30). In addition, ACT has been reported to have effects against carbon tetrachloride-induced hepatotoxicity (31). The aforementioned studies have suggested the potential roles of ACT in liver-related pathologies; however, the synergistic or antagonistic interactions between ACT and OXA, as well as the underlying mechanisms, have not yet been explored.

The present study aimed to investigate the synergistic and toxicity-reducing effects of ACT on OXA in HCC treatment using both *in vitro* and *in vivo* models (Fig. 1). Moreover, by combining transcriptomics and metabolomics analyses, the potential targets and mechanisms underlying the actions of ACT were explored and validated by western blotting. The present study not only provides insight into the synergistic application of Chinese medicinal herbs in HCC treatment, but also proposes novel therapeutic targets, thereby advancing the current understanding of HCC therapies and the theoretical and practical applications of traditional medicine in oncology.

Materials and methods

Cell lines and reagents. The human liver cancer HepG2 (RRID: CVCL_0027), human HCC PLC/PRF/5 cell line (RRID: CVCL_0485) and murine HCC Hepa1-6 cell line (RRID: CVCL_0327) were authenticated by short tandem repeat analysis and were provided by Procell Life Science and Technology Co., Ltd. All cell lines were authenticated within the last 3 years by Procell Life Science and Technology Co., Ltd. Mycoplasma-free cells were used for all experiments. ACT extracted from *Cistanche tubulosa* (Schenk) Wight (cat. no. 103200) was purchased from Yongjian Pharmaceutical Technology, with a purity >98%. OXA (cat. no. 100584) was from National Institutes for Food and Drug Control.

Cell culture. HepG2, PLC/PRF/5 and Hepa1-6 cell lines were cultured in Dulbecco's modified Eagle's medium (DMEM), minimum essential medium (MEM) (both from HyClone; Cytiva) and DMEM containing 10% fetal bovine serum (FBS; Corning Life Sciences), 100 U/ml penicillin and 100 μg/ml streptomycin, respectively. Cells were cultured at 37˚C in 100% humidity and 5% CO_2. Cells were dissociated to single cells using trypsin-EDTA upon reaching 80-90% confluence, followed by termination of enzymatic digestion with complete medium.

Cell treatment. A total of $5x10^3$ cells were cultured in a 96-well plate filled with complete medium for 48 h. OXA (1.56, 3.13, 6.25, 12.50, 25.00, 50.00, 75.00, 100.00 μM) and ACT (3.13, 6.25, 12.50, 25.00, 50.00, 100.00, 200.00, 400.00 μM) intervened three HCC cells (HepG2, PLC/PRF/5, Hepa1-6) for 48 h at 37˚C. Detection of the IC_{50} of HCC cells by Cell Counting Kit-8 (CCK-8) assay. HepG2 cells were grouped as follows: i) Control, untreated; ii) OXA (1.56, 3.13, 6.25, 12.50 and 25.00 μM); iii) ACT (6.25, 12.50, 25.00, 50.00 and 100.00 μM) and iv) OXA + ACT (1.56+6.25, 3.13+12.50, 6.25+25.00, 12.50+50.00 and 25.00+100.00 μM) at the same time. Hepa1-6 cells were grouped as follows: i) Control, untreated; ii) OXA, (1.56, 3.13, 6.25, 12.50 and 25.00 μM); iii) ACT (25.00, 50.00, 100.00, 200.00 and 400.00 μM) and iv) OXA + ACT (1.56+25.00, 3.13+50.00, 6.25+100.00, 12.50+200.00 and 25.00+400.00 μM) at the same time. The OXA/ACT concentration ratios were determined based on half-maximal inhibitory concentration (IC_{50}) values.

Cell viability assay. HepG2 and Hepa1-6 cells were incubated for 4 h in a 96-well plate with 10 μl/well CCK-8 reagent (Beijing Solarbio Science & Technology Co., Ltd.). Cell viability was measured using a multi-detection microplate reader (Multiskan™ FC; Thermo Fisher Scientific, Inc.) at 450 nm. CI of OXA combined with ACT was calculated using CompuSyn 1.0 (Biosoft) and the CI curve was drawn as previously described (32). CI=0.9-1.1, <0.9 and >1.1 indicated an additive effect, synergism and antagonism, respectively.

Cell invasion assay. Cell invasion was evaluated using a Transwell assay as previously described (33). The Matrigel® matrix (cat. no. 356234; lot no. 8155016; Corning, Inc.) was thawed at 4˚C and then diluted with serum-free DMEM at a 1:8 volume ratio for coating overnight at 37˚C. Transwell chambers. Cells ($1x10^5$) suspended in 200 μl high-glucose FBS-free DMEM were seeded in the upper chamber. High-glucose DMEM (600 μl) supplemented with 10% FBS was placed in the lower chamber. Following incubation for 48 h at 37˚C, cells on the upper surface were removed. Next, cells fixed for 30 min at room temperature using 95% ethanol, then stained for 30 min at room temperature with 0.1% crystal violet and observed under a light microscope (magnification, x100).

Cell migration assay. Cell migration was assessed using a wound healing assay as previously described (33). Cells were seeded in 6-well plates until they reached 100% confluence. After wounding with a 200-μl pipette tip and washing with PBS, cells were incubated in serum-free DMEM (HyClone; Cytiva) at 37˚C. Wound images at 0, 12, 24 and 48 h were captured under a light microscope (magnification, x200). Wound distance was expressed as ratio to the initial distance at 0 h.

Cell cycle analysis. Cells ($5x10^5$) were incubated in 6-well plates for 24 h at 37˚C in 5% CO_2 and were cultured for 4 h in serum-free DMEM. Cells were then digested with 0.25%

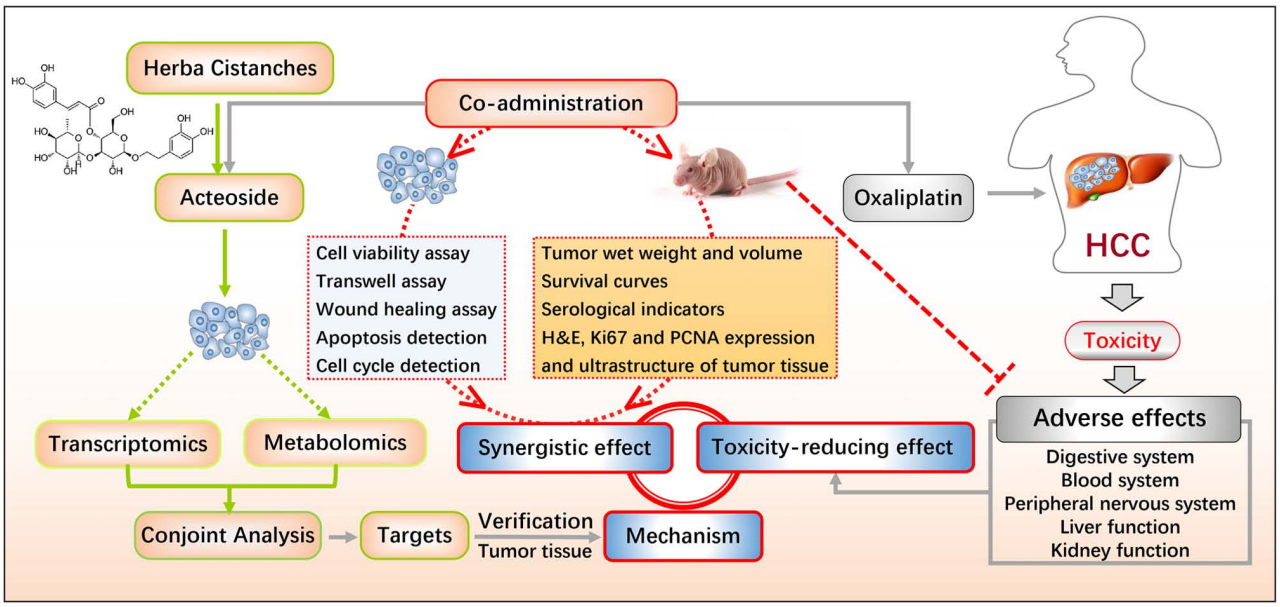

Figure 1. Workflow of the present study. H&E, hematoxylin and eosin; HCC, hepatocellular carcinoma; PCNA, proliferating cell nuclear antigen.

pancreatin. Following centrifugation at 1,000 x g for 5 min at room temperature, cells were suspended with PBS buffer to a concentration of 1-5x10^5 cells/ml. After PI and RNase A (cat. no. C1052, Beyotime biotechnology) staining at 37˚C away from light for 30 min, cells were subjected to flow cytometry using a flow cytometer (DXFLEX, Beckman, USA). FlowJo (version 10.6.2; Tree Star, Inc.) was used to analyze data.

Transcriptomics analysis. Total RNA of HepG2 cells was isolated using TRIzol® (Invitrogen; Thermo Fisher Scientific, Inc.) according to the manufacturer's instructions. Purity was determined using the NanoDrop ND-1000 (NanoDrop). RNA were reverse-transcribed by SuperScript™ II Reverse Transcriptase (Invitrogen, cat. 1896649, USA), which were used to synthesize U-labeled second-stranded DNAs with *E. coli* DNA polymerase I (NEB, cat.m0209, USA), RNase H (NEB, cat. no. m0297, USA) and dUTP Solution (Thermo Fisher, cat.R0133, USA). An A-base is then added to the blunt ends of each strand, preparing them for ligation to the indexed adapters. Each adapter contains a T-base overhang for ligating the adapter to the A-tailed fragmented DNA. Single- or dual-index adapters are ligated to the fragments, and size selection was performed with AMPureXP beads. After the heat-labile UDG enzyme (NEB, cat.m0280, USA) treatment of the U-labeled second-stranded DNAs, the ligated products are amplified with PCR. For each sample, 10 pM RNA was selected for sequencing library construction. The average insert size for the final cDNA library was 300±50 bp. At last, we performed the 2x150 bp paired-end sequencing (PE150) on an Illumina Novaseq™ 6000 (LC-Bio Technology CO., Ltd.) with a KAPA Stranded RNA-seq Library Prep kit (cat. no. KK8401; Illumina, Inc.) following the vendor's recommended protocol. The differentially expressed genes (DEGs) between control group and ACT group were selected by R package (version 4.0.2, cran.r-project.org/bin/windows/) (34). The sequencing data can be accessed at https://www.ncbi.nlm.nih.gov/sra/PRJNA 1219772.

Untargeted metabolomics analysis. Metabolomics analysis was performed by LC-Biotechnology. Briefly, six cell samples per group were randomly used for metabolomics analysis. Cell pre-processing was performed as previously described (35). HepG2 cell extracts were analyzed on a Triple TOF 5600 plus mass spectrometer (SCIEX). Quadrupole time-of-flight mass spectrometry was operated in negative and positive ion modes. Data were acquired in data independence initiative mode, with 60-1, 200 Da TOF mass and 0.56 sec total cycle. For each scan, 4-time bins were aggregated at an 11-kHz pulse frequency by monitoring a 40-GHz multi-channel thermal conductivity detector with four-anode/channel detection, dynamically excluded for 4 sec. The mass accuracy was calculated per 20 samples. A quality control sample (aliquots of all samples were mixed) was injected at the beginning to equilibrate the system and then every 10 samples to monitor the stability of the system. Kyoto Encyclopedia of Genes and Genomes (URL: http://www.genome.jp/kegg) enrichment analysis on transcript and metabolite profiles was conducted to explore the potential link between mRNA-metabolomics pathways (impact value >0.1) and DEGs. Data processing and analysis were performed as previously described (36).

Animals. A total of 50 male BALB/c nude mice (SPF grade; age, 5-6 weeks; weight, 18-22 g) were purchased from Beijing Huafukang Biotechnology Co., Ltd. (license no. SCXK 2019-0008), reared under standard environmental conditions (26-28˚C; relative humidity, 40-60%; 12/12-h light/dark cycle, with food and water provided ad libitum. All animal experiments were conducted following the ethical guidelines approved by the Experimental Animal Ethics Committee of the First Affiliated Hospital of Xinjiang Medical University (approval no. IACUC-20210301-179; Urumqi, China).

Mouse model. A xenograft mouse model was established by subcutaneously injecting HepG2 cells (1x10^7 cells/200 μl of 0.9% physiological saline) into the axillary region as

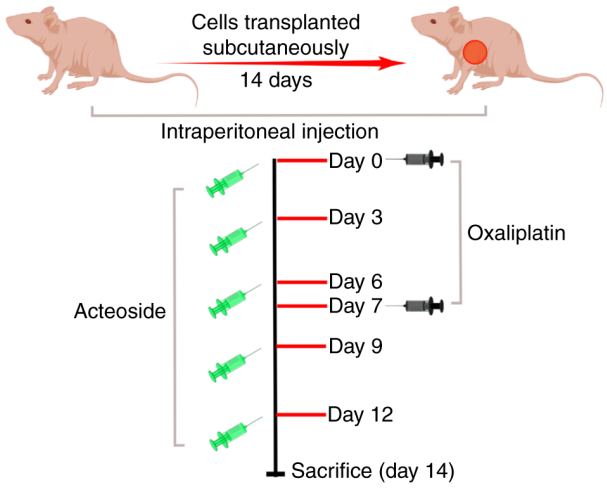

Figure 2. Schematic of the administration cycle.

previously described (33). A total of 2 weeks post-injection, mice with tumor volumes >100 mm^3 were randomly assigned to the following groups (n=11/group): i) Model group, receiving an equivalent volume of 5% glucose injection; ii) OXA group, administered 5 mg/kg OXA weekly; iii) ACT group, treated with 80 mg/kg ACT every 3 days; and iv) OXA + ACT group, receiving 5 mg/kg OXA weekly in combination with 80 mg/kg ACT every 3 days (Fig. 2). In addition, the control group was BALB/c nude mice not injected with HepG2 cells (n=6). OXA was dissolved in 5% glucose according to the manufacturer's instructions, while ACT was dissolved in sterilized water. All treatments were administered via intraperitoneal injection. All mice were weighed, and the tumor volume was calculated (0.5 a x b^2; a, length; b, width) every 3 days. After 2 weeks, six randomly selected mice in each group were anesthetized with sodium pentobarbital (50 mg/kg). Blood samples were collected from the eyeballs, followed by euthanasia via intraperitoneal injection of sodium pentobarbital (150 mg/kg). Tumor mass and small intestine tissues were isolated for further analysis. The tumor inhibition efficiency (%) was calculated as $(1-W_i/W_m)$ x100, where W_i is the mean tumor weight in each treatment group, and W_m is the mean tumor weight in the model group. Coefficient of drug interaction (CDI) was used to determine the interaction of OXA + ACT, calculated as AB/(A x B), where AB was the ratio of the tumor growth efficiency (W_i/W_m) in the two-drug combination group to the control group, and A or B was the ratio of the tumor growth efficiency in a single drug group to the control group (37). CDI values of <1, =1 and >1 indicated synergism, additive effects and antagonism, respectively. CDI <0.7 indicated significant synergistic effects. To evaluate the roles of OXA + ACT on the survival of HepG2 tumor-bearing mice using Kaplan-Meier curve, the remaining five mice in each group received the same regimen for another 60 days. Humane endpoints were as follows: i) Tumor volume exceeded 2,000 mm^3; b. Tumor diameter exceeded 20 mm; c. Rapid or continuous weight loss of more than 20% within 72 h; d. Tumor ulceration or necrosis resulted in skin rupture or persistent exudation for more than 48 h; e. Significant abdominal distension or ascites burden exceeding 10% of body weight, with an appearance similar to that of a pregnant mouse compared to age-matched controls; f. The survival observation period was set at 60 days, and all mice were euthanized at the end of this phase. Sodium pentobarbital (150 mg/kg) was administered via intraperitoneal injection to induce respiratory arrest. The survival time of mice in each group was recorded to construct survival curves using Graphpad prism 8.0.

Hematoxylin and eosin (H&E) staining, immunofluorescence staining and ultrastructural analysis of tumor tissues. Tumor tissue sections were stained with H&E for histological evaluation, as previously described (38). Images were captured using a light microscope and percent of tumor necrotic area of total tumor from mice was semi-quantified by ImageJ (version1.54g) software (National Institutes of Health). Ki67 and proliferating cell nuclear antigen (PCNA) were evaluated as tumor cell proliferation markers (39) detected in tumor tissue sections to assess cell viability. Incubate sections (thickness, 0.2-0.3 cm) were fixed in methanol for 30 min at room temperature, rinsed with xylene and dehydrated by gradient ethanol. Immerse the slides in EDTA antigen retrieval buffer (pH 8.0) and maintain at a sub-boiling temperature for 8 min, standing for 8 min and then followed by another sub-boiling temperature for 7 min. Wash three times with PBS (pH 7.4) in a Rocker device, 5 min each. Add 3% BSA (Wuhan Servicebio Technology Co., Ltd, China, https://www.servicebio.cn/) to block non-specific binding for 30 min at room temperature. The primary anti-PCNA (1:400; cat. no. GB11010-100) and anti-Ki67 (1:500; cat. no. GB121141-100, both Wuhan Servicebio Technology Co., Ltd, China) was added at 4˚C overnight. Following three washes with PBS, the Alexa Fluor 488-labeled goat anti-mouse IgG secondary antibody (1:500; cat. no. GB25301, Wuhan Servicebio Technology Co., Ltd.) and Cy3-labeled goat anti-rabbit IgG secondary antibody (1:500; cat. no. GB21303, Wuhan Servicebio Technology Co., Ltd, China) was added at room temperature for 50 min. Sections were stained with DAPI at room temperature for 10 min. Then, the tumor tissue sections are observed using a fluorescence microscope (Nikon Eclipse C1, Nikon) at a magnification of x40. A total of three random fields of view were selected for each section. The fluorescence intensities of Ki67 and PCNA were calculated using ImageJ 1.45 (National Institutes of Health) as follows: Fluorescence intensity (%)=fluorescence-stained area/DAPI-stained area x100.

Fresh tumor tissue was fixed with 2.5% glutaraldehyde (cat. no. G1102, Wuhan Servicebio Technology Co., Ltd, China) for 24 h at 4˚C. Tissue was embedded in EMBed 812, and then keep in 37˚C oven overnight. The resin blocks were cut to 60-80 nm thin on the ultra-microtome, and the tissues were fished out onto the 150 meshes cuprum grids with formvar film (cat. no. HT7700, Hitachi Ltd., Japan). Sections were stained with 2% uranium acetate saturated alcohol solution for 8 min at room temperature, rinsed in 70% ethanol (cat. no. 100092183, Sinaopharm Group Chemical Reagent Co. Ltd., China) and ultra-pure water three times. 2.6% Lead citrate avoid CO_2 staining for 8 min, and then rinsed with ultra-pure water for 3 times. Then, the tumor tissue sections are sent to the electron microscopy room at Xinjiang Medical University for observation using a transmission electron microscope (JEM-100CX II TEM, JEOL Ltd.).

ELISA. Whole blood was allowed to set at room temperature for 1 h, centrifuged at 1,509.3 g at 4˚C for 10 min, and serum was collected. ELISA was performed to detect serum levels of IL-6, hypersensitive C-reactive protein (hs-CRP), α fetoprotein (AFP) and TNF-α using Human hs-CRP ELISA Kit (cat. no. JL10346), Human aFP ELISA Ki (cat. no. JL40021) and Human TNF-α ELISA Kit (cat. no. JL10484), according to the manufacturer's instructions (Shanghai Jianglai Biotechnology Co., Ltd.). All the tests were performed at least in triplicate.

Histological, hematological, neurological and biochemical analyses. H&E staining was performed on the intestinal tissue sections to evaluate the effects of ACT on OXA-induced digestive toxicity, as aforementioned. White blood cells (WBCs), red blood cells (RBCs) and platelets (PLTs) were counted to assess the effects of ACT on OXA-induced hematological toxicity. In addition, the effects of ACT on OXA-induced OXIN were evaluated by measuring the paw withdrawal mechanical threshold (PWMT) using Von Frey hairs. Levels of serum alanine aminotransferase (ALT; cat. no. C009-2-1), aspartate aminotransferase (AST; cat. no. C010-2-1), alkaline phosphatase (AKP; cat. no. A059-2-2), lactate dehydrogenase (LDH; cat. no. A020-2-2), creatinine (CRE; cat. no. C011-2-1) and blood urea nitrogen (BUN; cat. no. C013-2-1) were detected according to the manufacturer's instructions (Nanjing Jiancheng Bioengineering Institute, Ltd.) to assess the OXA-induced hepatotoxicity and nephrotoxicity in the presence of ACT.

Western blotting. Protein of tumor tissue was extracted with RIPA lysis buffer (Thermo Fisher Scientific, Inc.) and protein concentration was detected using the bicinchoninic acid assay method. A total of 10 μg/lane protein was separated by 10% SDS-PAGE, blocked in 5% non-fat milk for 1h at 4˚C, then transferred to PVDF membrane (Merk Millipore, cat. no. R1CB35759) and incubated with appropriate primary antibodies at 4˚C overnight and secondary antibodies at room temperature for 4 h. The PVDF membrane was rinsed with TBST (containing 0.1% Tween-20). The primary antibodies β-actin (cat. no. bs-0061R; 1:5,000), AKT1 (cat. no. bsm-52010R; 1:500), phosphorylated (p)-AKT1 (cat. no. bs-5194R; 1:500), PIK3R1 (cat. no. bs-0128R; 1:500), p-PIK3R1 (cat. no. bs-6417R; 1:500), PRKCA (cat. no. bsm-54393R; 1:500), INPP5D (cat. no. bs-3567R; 1:500), PTEN (cat. no. bsm-33319M; 1:500). and the secondary antibodies goat anti-rabbit IgG H&L (cat. no. bs-0295G; 1:5,000) and anti-mouse IgM, HRP conjugated (cat. no. bs-0368G-HRP; 1:5,000) purchased from Beijing Bioss Biotechnology Co., Ltd (http://bioss.com.cn/). The primary antibodies PLCB4 (cat. no. DF2564; 1:500), INPP4B (cat. no. DF7975; 1:1,000) and PIKFYVE (cat. no. DF8707; 1:1,000) purchased from Shanghai Fushen Biotechnology Co., Ltd (https://www.fsbio-mall.com/). Blots were visualized using an enhanced chemiluminescence (Hefei White Shark Biotechnology Co., Ltd. cat. no. 1027a01), and relative intensity was semi-quantified by ImageJ (version1.54g) software (National Institutes of Health) and normalized to the intensity of β-actin. Antibodies against PLCB4, INPP4B and PIKFYVE were from Affinity Biosciences. All other antibodies were from Boaosen Biotechnology.

Statistical analysis. All experiments were performed in triplicate. GraphPad Prism 5.0 and CompuSyn software were used to calculate IC_{50} and CI values, respectively. SPSS 22.0 (IBM Corp.) was used for statistical analyses. Data are presented as the mean ± standard deviation. Comparisons were performed using one-way ANOVA followed by Bonferroni's post hoc test. $P<0.05$ was considered to indicate a statistically significant difference.

Results

ACT enhances OXA-induced antitumor effects on HCC in vitro. OXA and ACT were used to treat liver cancer cell lines (PLC/PRF/5, HepG2 and Hepa1-6) for 48 h. For OXA treatment (Fig. S1A), the IC_{50} values in HepG2, PLC/PRF/5 and Hepa1-6 cells were 15.81, 22.56 and 16.79 μM, respectively. For ACT (Fig. S1B), the IC_{50} values in HepG2, PLC/PRF/5 and Hepa1-6 cells were 71.72, 74.74 and 241.40 μM, respectively. HepG2 cells showed the greatest sensitivity (lowest IC_{50} value) and were selected as the most suitable liver cell line for animal studies.

Validation and optimal dosage of ACT + OXA for synergistic inhibition in HepG2 and Hepa1-6 cells. The CI value for ACT + OXA was <0.9, suggesting this combination synergistically inhibited the viability of HepG2 and Hepa1-6 cells (Figs. S2 and S3). In HepG2 cells, the CI value for the 50 μM ACT + 12.5 μM OXA treatment group was 0.25±0.41, which was lower than that of other dose combinations (Table SI). In Hepa1-6 cells, 200 μM ACT + 12.5 μM OXA yielded the lowest CI value (0.07±0.01; Table SII). Regarding safety, ACT/OXA concentration ratios of 50:12.5 and 200:12.5 μM were selected for subsequent experiments on HepG2 and Hepa1-6 cells, respectively.

ACT + OXA synergistically inhibits viability, invasion, migration and cell cycle progression of HepG2 and Hepa1-6 cells. Cell viability in OXA and/or ACT-treated groups was significantly decreased compared with that in the control group (Figs. 3A and 4A). In addition, cell viability in the OXA + ACT group showed a significant decrease compared with the OXA and ACT groups. The Transwell assay showed cell invasion was decreased in the OXA compared with that in the control group, and in the OXA + ACT group compared with that in OXA group (Figs. 3B and 4B).

The wound healing assay showed that the wound size in the OXA + ACT group increased, whereas in the control, OXA, and ACT groups, get smaller. (Figs. 3C and 4C). After 48 h, the wound size in the OXA + ACT group was significantly increased compared with that in the OXA and ACT groups. This finding suggested that cell migration was reduced in the OXA + ACT group compared to the other groups (Figs. 3D and 4D).

The rate of early cell apoptosis was increased in the OXA and/or ACT groups compared with that in the control group. The early apoptotic rate of the OXA + ACT group was higher than that in the OXA and ACT groups (Figs. 3E and G, and 4E and G).

In the OXA + ACT group, the proportion of G_0/G_1 phase cells showed a significant increase compared with that in the

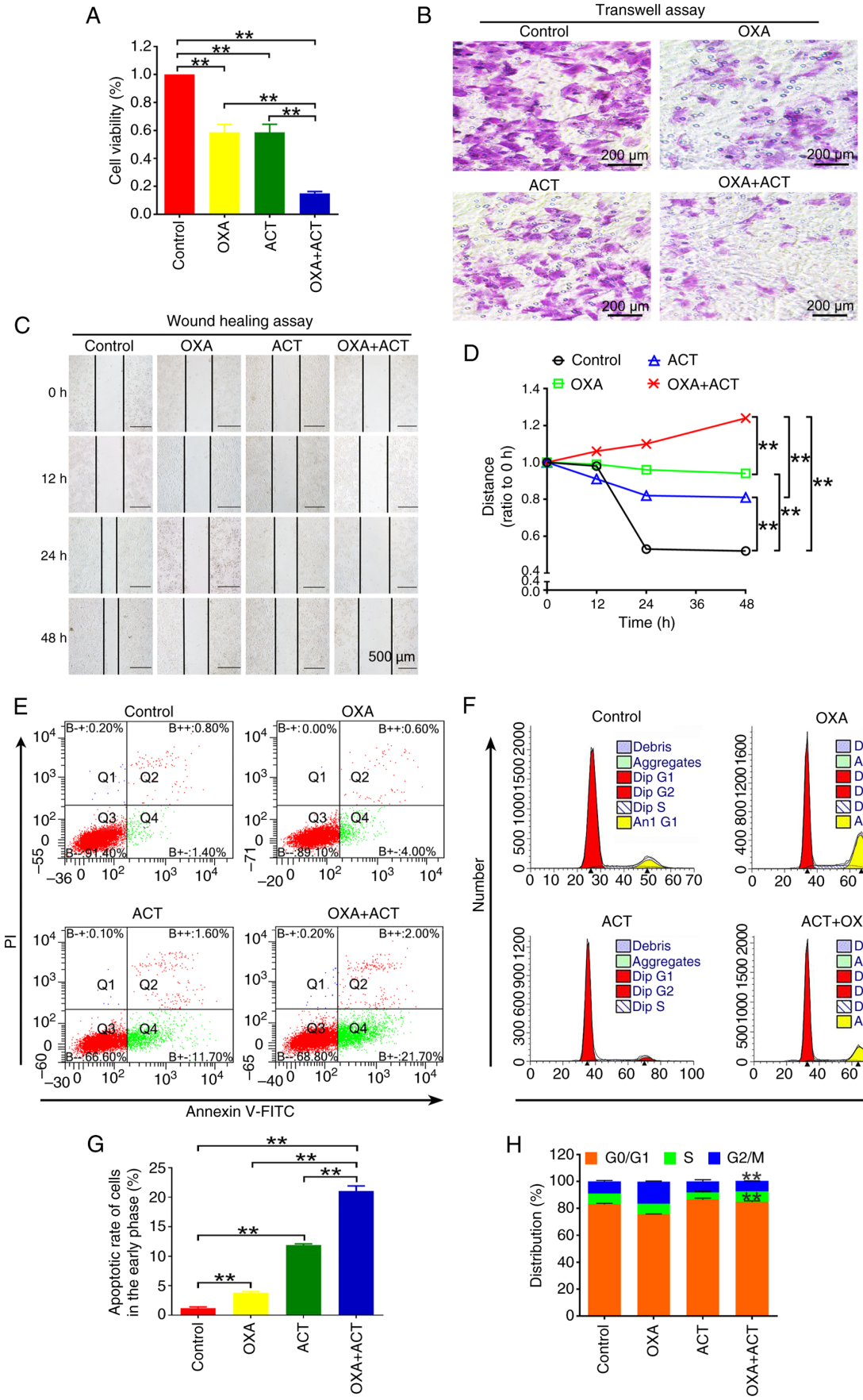

Figure 3. ACT enhances the antitumor roles of OXA in the HepG2 cell line. (A) Cell proliferation assay. results. (B) Representative images (magnification, x200) of cell invasion in each group, as determined by Transwell assay. (C) Representative images (magnification, x40) of cell migration, as detected by wound healing assay. (D) Scratch distances of cells in each group at different time points. (E) Distribution of apoptotic cells. (F) Distribution of HepG2 cells in the cell cycle. (G) Statistical analysis of early apoptotic cells (Q4). (H) Statistical analysis of the percentage of cells in each phase. **P<0.01 vs. OXA. ACT, acteoside; OXA, oxaliplatin.

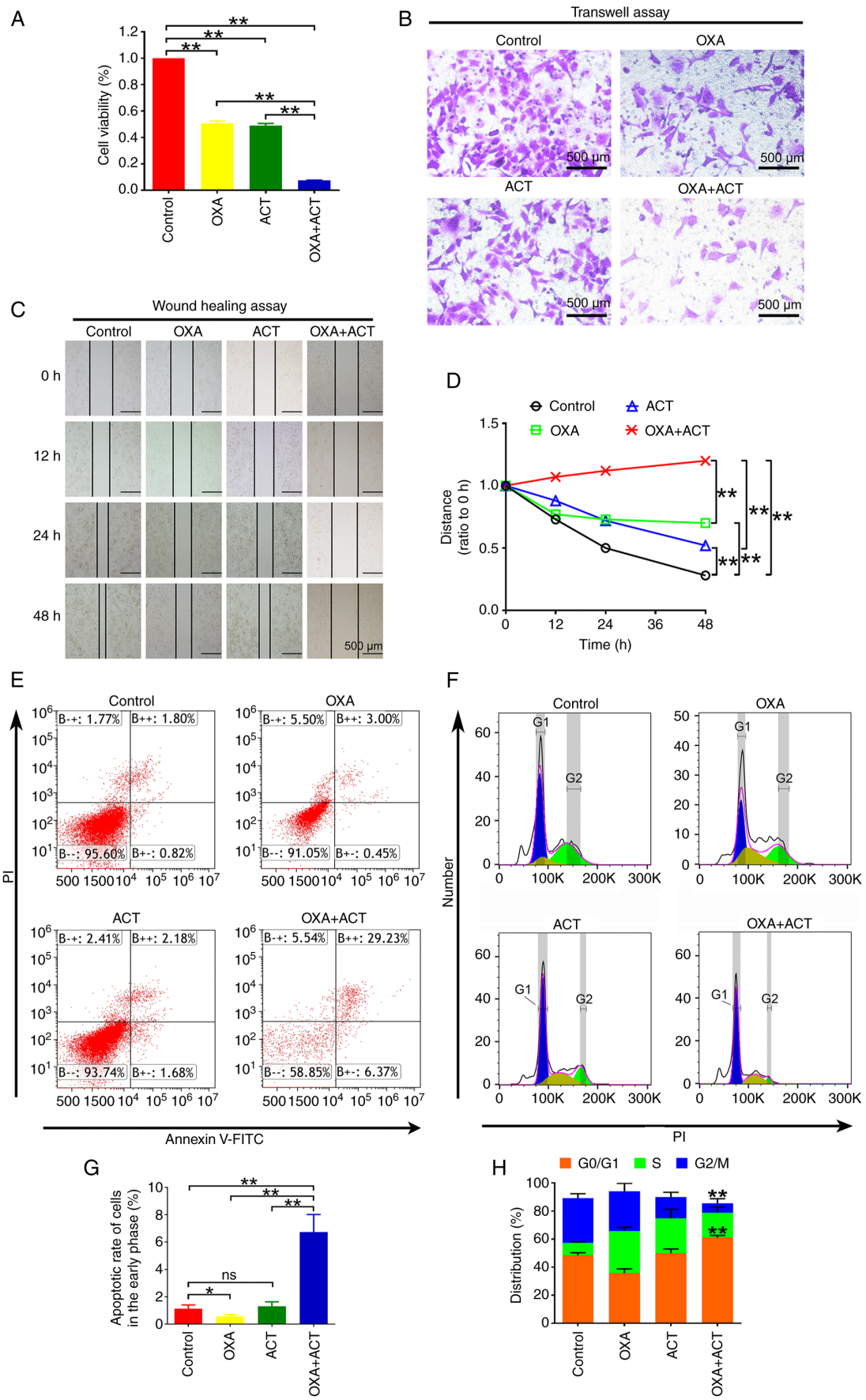

Figure 4. ACT enhances the antitumor roles of OXA in the Hepa1-6 cell line. (A) Cell proliferation assay. results. (B) Representative images (magnification, x200) of cell invasion in each group, as determined by Transwell assay. (C) Representative images (magnification, x40) of cell migration, as detected by wound healing assay. (D) Scratch distances of cells in each group at different time points. (E) Distribution of apoptotic cells. (F) Distribution of HepG2 cells in the cell cycle. (G) Statistical analysis of early apoptotic cells (Q4). (H) Statistical analysis of the percentage of cells in each phase. *P<0.05, **P<0.01, compared with OXA group in H. ns, not significant; ACT, acteoside; OXA, oxaliplatin.

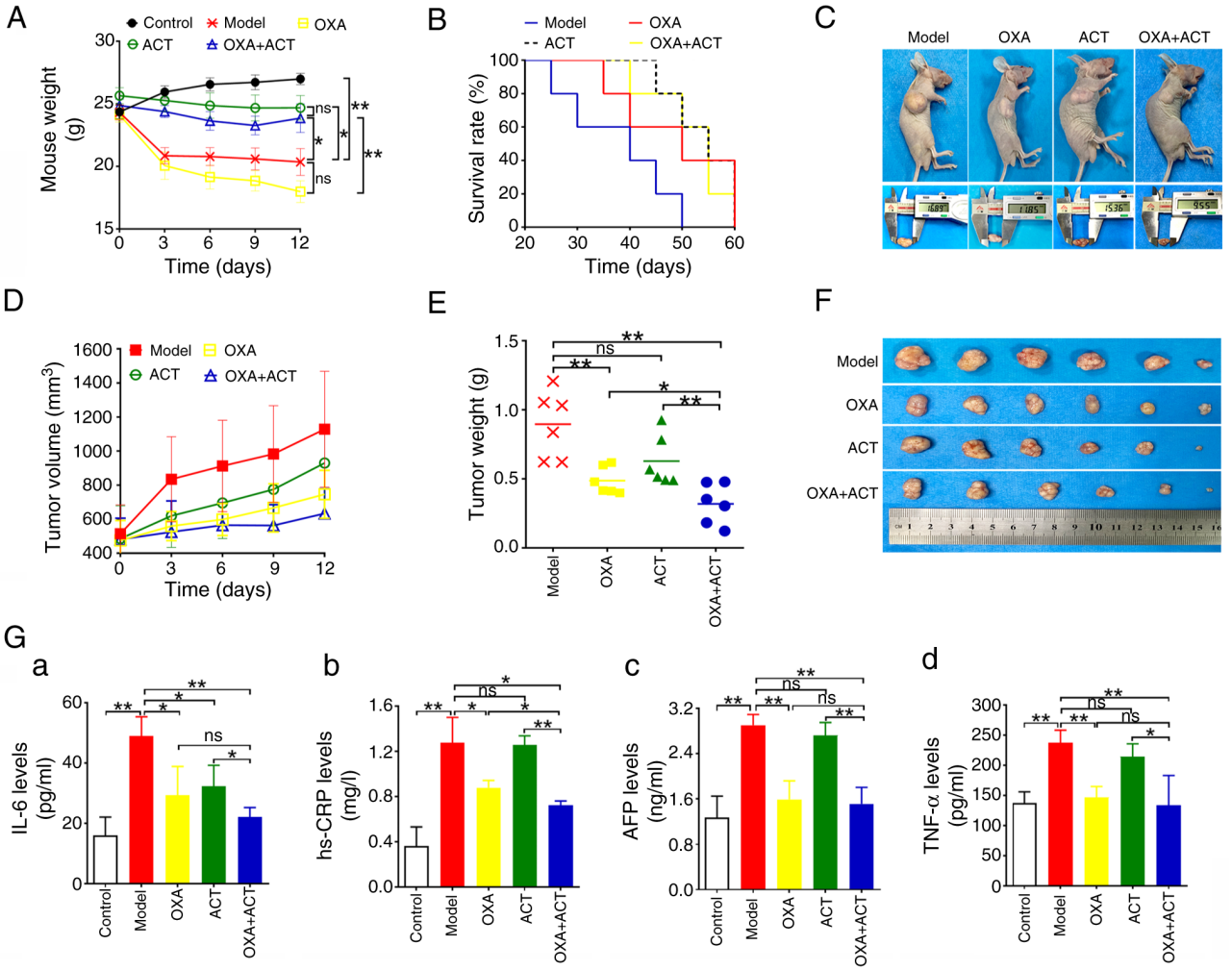

Figure 5. ACT enhances the antitumor roles of OXA in hepatocellular carcinoma *in vivo*. (A) Weight change of the nude mice. (B) Survival rate of HepG2 model mice. (C) HepG2 model mice. (D) Tumor volume and (E) weight changes in HepG2 tumor-bearing mice. (F) Isolated tumor masses in each group. (G) Serum (a) IL-6, (b) hs-CRP, (c) AFP and (d) TNF-α levels of nude mice in each group. *P<0.05, **P<0.01. ns, not significant; ACT, acteoside; OXA, oxaliplatin; hs-CRP, hypersensitive C-reactive protein; AFP, α fetoprotein.

OXA group, together with a significant decrease in the proportion of S phase cells (Figs. 3F and H and 4F and H). These results indicated that OXA + ACT could arrest cells in G_0/G_1 phase.

ACT enhances the antitumor effects of OXA on HCC in vivo. All six mice in each group survived without any fatalities. The body weight of mice in the OXA + ACT group showed a decrease within 9 days of the intervention and increased after day 9. Notably, the body weight of mice in the OXA + ACT group was significantly increased compared with that of mice in the OXA group on day 12 (Fig. 5A). The maximum diameter and volume of the tumors detected during the 2-week treatment phase were 17.48 mm and 1,997.32 mm^3, respectively. Tumor volume in the OXA and OXA + ACT groups was decreased compared with that in the model group after 12 days, although the difference was not significant (Fig. 5D). In the model group, the first nude mouse death occurred on day 25, and all nude mice died within 50 days. By contrast, in the OXA, ACT and OXA + ACT groups, the first mouse death was observed on days 35, 45 and 40, respectively. There was no significant difference in median survival time between the OXA + ACT group, and the model or OXA groups (Fig. 5B). Mice used for 60-day survival analysis in each group euthanized due to tumor growth, tumor ulceration and nutritional depletion (Table SIII).

The tumor volume in the OXA + ACT group was lower than that in the model group (Fig. 5C, D and F). Furthermore, compared with in the OXA group, tumor weight was significantly decreased in the OXA + ACT group (0.319±0.147 vs. 0.487±0.099 g; Fig. 5E; Table SIV). Moreover, the CDI of the OXA + ACT group was 0.93, indicating a synergistic effect of ACT and OXA in HCC.

IL-6, hs-CRP, TNF-α and AFP levels were significantly decreased in the OXA and OXA + ACT groups compared with those in the model group (Fig. 5G). In addition, serum hs-CRP levels were significantly decreased in the OXA + ACT group compared with those in the OXA group and serum IL-6, hs-CRP, TNF-α and AFP levels were significantly decreased in the OXA + ACT group compared with those in the ACT group.

In each group, the nuclei of the tumor necrosis area were fragmented, exhibited pyknosis or were absent while the viable tumor survival area showed intact nuclei with clear boundaries (Fig. 6A). Compared with in the model group, tumor necrosis in the OXA and/or ACT groups was significantly increased (Fig. 6B). Furthermore, tumor necrosis in the OXA + ACT

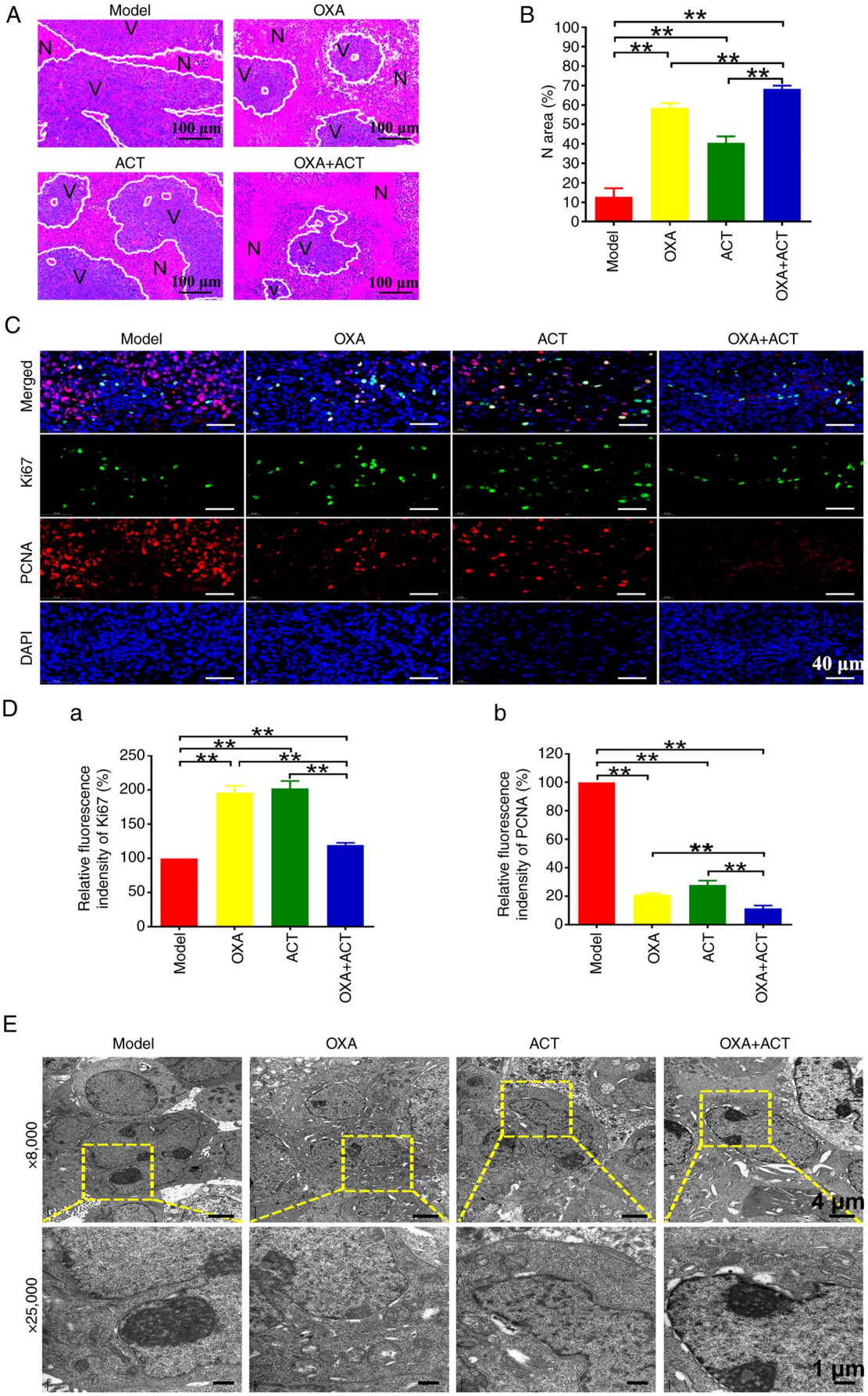

Figure 6. ACT enhances antitumor effects of OXA on hepatocellular carcinoma *in vivo*. (A) Hematoxylin and eosin staining of tumor tissues (magnification, x100). (B) Proportion of N area. (C) Immunofluorescence staining (magnification, x40) of Ki67 (green) and PCNA (red) expression. Blue, nucleoli. (D) Relative fluorescence intensity of (a) Ki67 and (b) PCNA. (E) Ultrastructure of tumor tissue sections. **P<0.01. ACT, acteoside; OXA, oxaliplatin; N, necrotic; V, viable; PCNA, proliferating cell nuclear antigen.

group showed a significant increase compared with that in the OXA and ACT groups.

The Ki-67 levels in tumor tissues in the OXA and/or ACT groups were significantly increased compared with those in the model group, whereas those in the OXA + ACT group were significantly decreased compared with those in the OXA group. By contrast, PCNA levels in the OXA and/or ACT groups showed a significant decrease compared with those in the model group, and the OXA + ACT group showed a further significant decrease in PCNA levels compared with in the OXA and ACT groups (Fig. 6C and D).

Regarding the results of transmission electron microscopy, heteromorphic nuclei, partially depressed nuclear membranes, nuclear notches, binucleated cells and depleted organelles were observed in the model group (Fig. 6E). The mitochondrial ridges were dissolved, swollen and vacuolized in the tumor cells in the OXA group. The tumor cells in the ACT group showed lysed nuclear membranes, heteromorphic flocculent substances and lysed mitochondrial ridges. The combination of OXA + ACT resulted in disintegration of cell membranes, widening of the perinuclear spaces, cavitation of mitochondria, complete dissolution of the outer mitochondrial membranes and rough endoplasmic reticula with degranulation and marked expansion.

ACT alleviates OXA-induced toxicity in vivo. The small intestinal tissues in both the control and model groups exhibited regular pathological morphology, with intact intestinal villi and clear boundaries (Fig. 7A). By contrast, the small intestinal villi in the OXA group were damaged, with some villi ruptured and unclear boundaries. However, the OXA + ACT group showed alleviated damage, with better preserved intestinal villi compared with model group. The PWMT value in the OXA + ACT group was significantly higher than that in the model group, and significantly lower than that in the OXA group (Fig. 7B). Furthermore, compared with model group, WBC, RBC and PLT counts in the OXA group were significantly reduced (Fig. 7C), whereas these values were increased in the OXA + ACT group, particularly WBC and RBC counts. Compared with in the model group, the OXA group showed elevated levels of AST and decreased levels of AKP. The OXA + ACT group exhibited significantly lower AST and LDH levels compared with those in the OXA group. There was no significant change in ALT levels between groups (Fig. 7D). In addition, CRE levels in the model group were significantly higher than those in the control group, whereas CRE levels in the OXA + ACT group lower than those in the model group. BUN levels in the OXA group were significantly higher than those in the model group (Fig. 7E), whereas BUN levels in the OXA + ACT group were significantly lower than those in the OXA group (Fig. 7E).

ACT inhibits HCC progression by affecting multiple signaling pathways in vitro. Principal component analysis showed that the mRNA expression data of the HepG2 cells in the control and the ACT group were distinguishable (Fig. 8A and B). Compared with in the control group, 7,205 DEGs, including 3,010 upregulated and 4,195 downregulated genes, were screened in the ACT group (Fig. 8C and D). These data indicated that ACT may inhibit HCC progression by downregulating multiple signaling pathways. The volcano plots demonstrated 235 upregulated and 16 downregulated metabolites in the ACT group (Fig. 8E). Cluster analysis indicated 16 significant differentially expressed secondary metabolites between the control group and the ACT group (Fig. 8F and G). The top 20 enriched pathways in positive ion mode including 'phosphatidylinositol signaling system', 'inflammatory mediator regulation of TRP channels', 'inositol phosphate metabolism' and 'amino sugar and nucleotide sugar metabolism', as well as 'aldosterone synthesis and secretion'. Additionally, there were 20 enriched pathways in negative ion mode, including 'neuroactive ligand-receptor interaction', 'serotonergic synapse', 'protein digestion and absorption', 'amino sugar and nucleotide sugar metabolism' and 'glycerolipid metabolism' (Fig. 8H).

Table I. Potential target genes involved in the phosphatidylinositol signaling system.

Gene	Protein product	UniProt ID
AKT1	AKT serine/threonine kinase 1	B0LPE5
PIK3R1	PI3K	P27986
PLCB4	Phospholipase C β4	Q15147
PRKCA	Protein kinase Cα	P17252
PTEN	PTEN	P60484
INPP4B	INPP4 type II B	O15327
INPP5D	INPP5D	Q92835
PIKFYVE	PIKFYVE	Q9Y2I7

ACT inhibits the phosphatidylinositol signaling system in vivo. Following mRNA-metabolomics integration analysis through signal pathways, eight target genes/proteins involved in 'phosphatidylinositol signaling system' were screened, including AKT1, PIK3R1, PLCB4, PRKCA, PTEN, INPP4B, INPP5D and PIKFYVE (Table I and Fig. 9). As determined by western blotting, the protein expression levels of p-AKT1, AKT1, p-PIK3R1 p-PIK3R1/PIK3R1 and PRKCA showed a significant decrease in the OXA compared with those in the model group, whereas p-AKT1/AKT1, PLCB4, PTEN, INPP4B and INPP5D protein expression levels showed a significant increase. AKT1, p-PIK3R1 and PIK3R1 protein expression levels were significantly decreased in the ACT group compared with those in the model group, whereas PTEN, INPP4B and INPP5D protein expression levels showed a significant increase. In addition, compared with those in the OXA group, a significant increase was observed in p-AKT1, AKT1, p-AKT1/AKT1, p-PIK3R1, INPP4B and INPP5D protein expression levels in the OXA + ACT group. Moreover, compared with those in the ACT group, a decrease in AKT1, p-PIK3R1, and an increase in INPP4B and INPP5D protein expression levels were observed in the OXA + ACT group. Changes in both p-AKT1 and AKT1, p-PIK3R1 and PIK3R1 may be the result of the intervention of OXA and ACT, which led to an increase in the necrotic areas of the tumor tissues, resulting in changes in their protein content. The above results show that OXA+ACT co-administration up-regulated the expression of oncogene INPP4B/PTEN through the multi-signaling pathway in

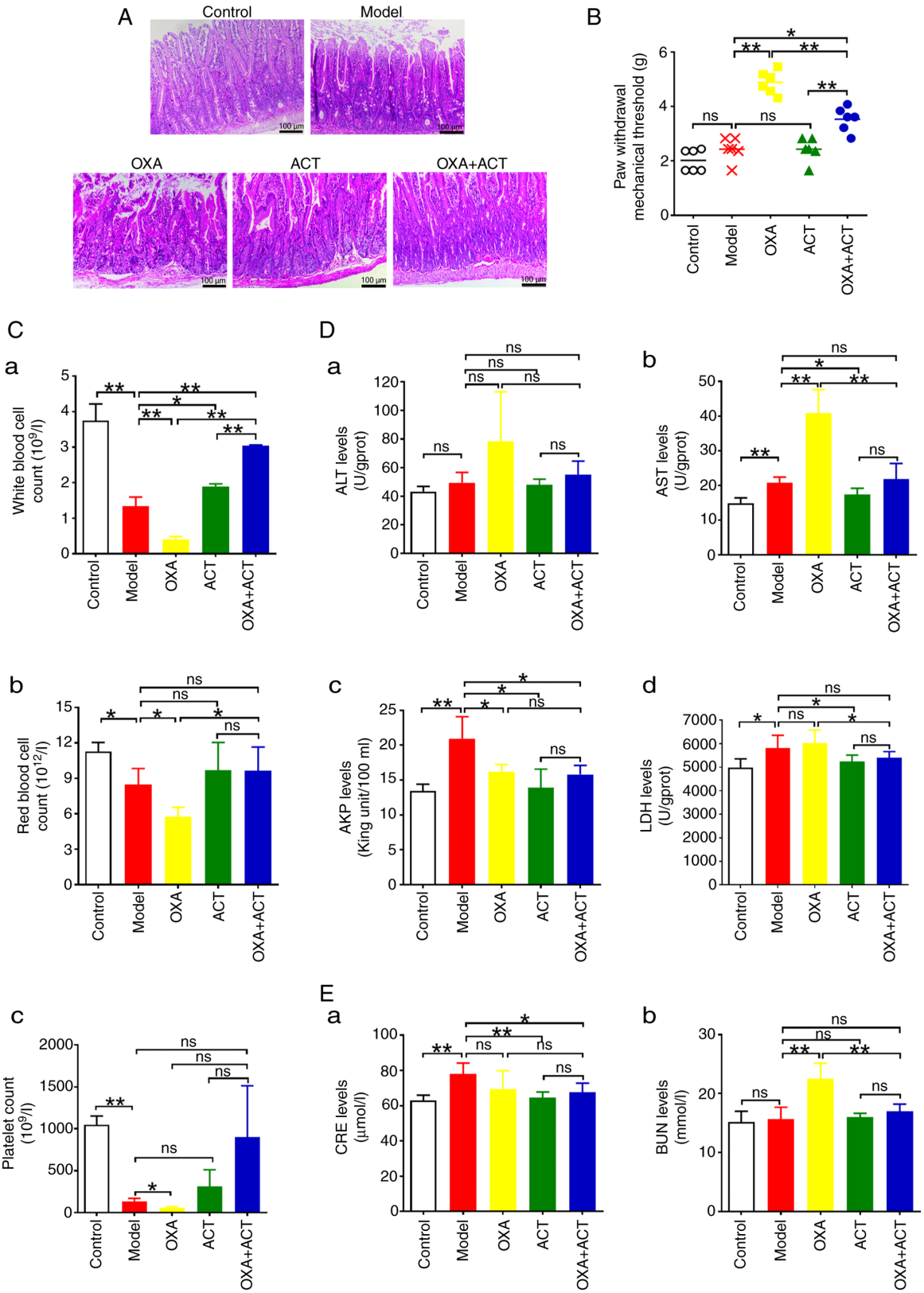

Figure 7. ACT alleviates OXA-induced toxicities *in vivo*. (A) Hematoxylin and eosin staining of the small intestinal tissues in each group of mice (magnification, x100). (B) Paw withdrawal mechanical threshold. (C) (a) White and (b) red blood cell, and (c) platelet count. (D) (a) ALT, (b) AST, (c) AKP and (d) LDH levels associated with OXA-induced hepatotoxicity. (E) Levels of (a) CRE and (b) BUN associated with OXA-induced nephrotoxicity. *P<0.05, **P<0.01. ns, not significant; ACT, acteoside; OXA, oxaliplatin; ALT, alanine aminotransferase; AST, aspartate aminotransferase; AKP, alkaline phosphatase; LDH, lactate dehydrogenase; CRE, creatinine; BUN, blood urea nitrogen.

the phosphatidylinositol signaling system inhibiting the PI3K(PIK3R1)/AKT signaling pathway to play a synergistic role in OXA to exert an anti-HCC effect while alleviating oxaliplatin-induced toxicity.

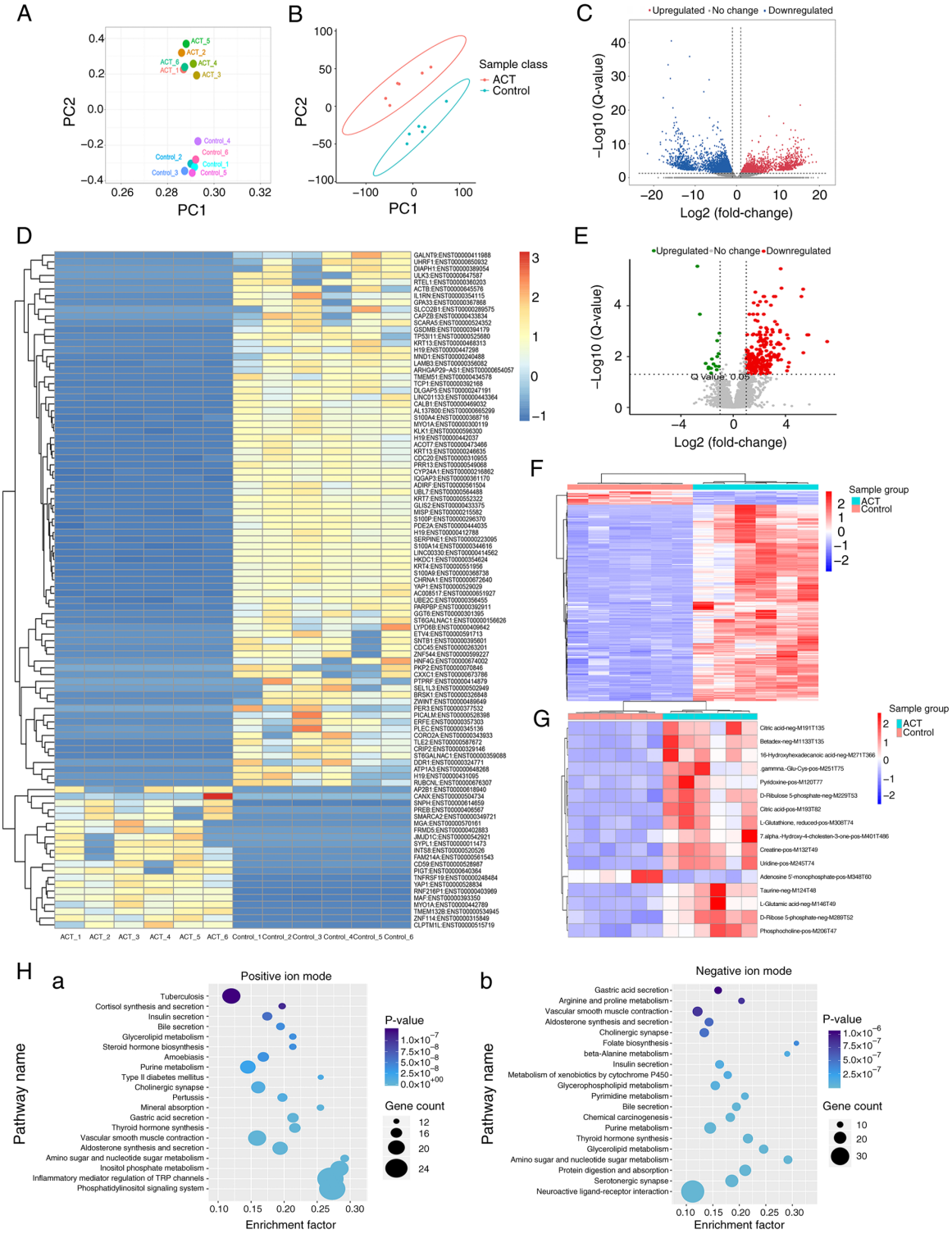

Figure 8. Transcriptomics and untargeted metabolomics analyses of ACT-treated HepG2 cells. (A) PCA plot of HepG2 cells. (B) PCA classification of control and ACT groups as positive and negative patterns, respectively. (C) Volcano plot of DEGs. (D) Heat map of DEGs in two groups. (E) Volcano plot and (F) heat map of differentially expressed metabolites. (G) Significantly differentially expressed secondary metabolites. (H) Kyoto Encyclopedia of Genes and Genomes enrichment analysis of DEGs; top 20 pathways detected under (a) positive ion mode and (b) negative ion mode are presented. ACT, acteoside; PCA, principal component analysis; DEG, differentially expressed gene.

Discussion

Cancer cell invasion and migration are the primary biological characteristics of intermediate and advanced cancers. It has been shown that ACT can restrain malignant cancer cell proliferation, invasion and migration through multiple targets and signaling pathways (40,41). In the present study, as determined by Transwell and wound healing assays, it was confirmed that ACT + OXA synergistically restrained HepG2 and Hepa1-6 cell invasion and migration. Additionally, ACT could promote OXA-induced early apoptosis of HepG2 and Hepa1-6 cells. Therefore, it could be inferred that ACT exerted its effects

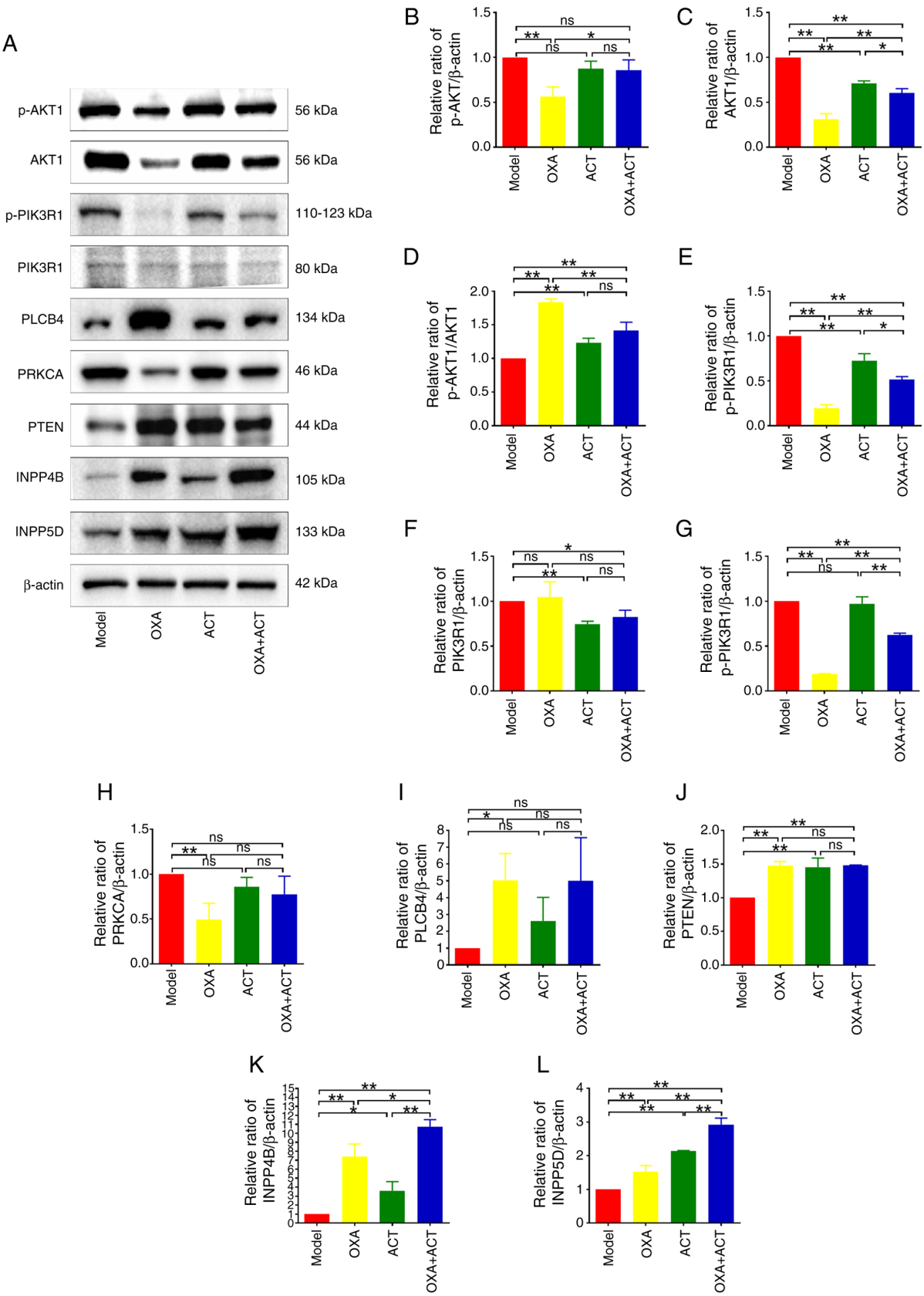

Figure 9. Effects of OXA + ACT on protein expression in the HepG2 model mice. (A) Western blot analysis. Effects of ACT + OXA on (B) p-AKT1, (C) AKT1, (D) p-AKT1/AKT1, (E) p-PIK3R1, (F) PIK3R1, (G) p-PIK3R1/PIK3R1, (H) PRKCA, (I) PLCB4, (J) PTEN, (K) INPP4B and (L) INPP5D protein levels in HepG2 model mice. *P<0.05, **P<0.01. ns, not significant; ACT, acteoside; OXA, oxaliplatin; p-, phosphorylated.

during the initial stage of the evolution of HCC, which may provide a basis for the prevention of HCC. Furthermore, it was shown that ACT + OXA inhibited HepG2 and Hepa1-6 cell proliferation and arrested cell cycle progression in G_1

phase. These data indicated that ACT may serve as a tumor suppressor in the early phase of HCC cell cycle.

The HepG2 cell line was selected to establish a mouse model for *in vivo* studies due to its sensitivity, as assessed by IC_{50}. The results revealed that ACT presented synergistic effects on OXA against HCC. Pathological morphology and tumor tissue ultrastructure showed that ACT increased OXA-induced necrosis and aggravated the ultrastructural injuries of tumor tissue. As Ki-67 is associated with cancer cell proliferation (42), it was hypothesized that the anti-cancer agents may inhibit cancer growth by downregulating Ki-67 expression. In the current study, immunofluorescence revealed that Ki67 expression in the OXA + ACT group showed a significant increase compared with that in the model group. However, the Ki67 levels in the OXA + ACT group were significantly decreased compared with those in the OXA group. Additionally, PCNA, a biomarker of cell proliferation that serves an important role in DNA replication, is upregulated in proliferating tumor cells and associated with malignant tumor progression (43-46). The present study demonstrated that compared with OXA alone, OXA + ACT inhibited tumor cell proliferation.

OXA exerts anti-cancer effects by inserting platinum atoms into the double-stranded DNA of tumor cells, but it also has side effects for patients (47). Generally, the main adverse events associated with OXA include toxicity in the digestive, blood and peripheral nervous systems, as well as in the liver and kidney. Gastrointestinal injury, one of the common OXA-induced adverse events, manifests as nausea, vomiting, diarrhea and abdominal pain (48,49). In the present study, small intestinal villi in the OXA group were damaged and the boundaries were blurred. However, OXA + ACT could attenuate the injuries of the small intestinal villi. These data suggested that ACT could alleviate gastrointestinal toxicities caused by OXA. Hematological toxicity is also a typical adverse event caused by OXA, which manifests as anemia, leukopenia and thrombocytopenia (50,51). The data of the present study demonstrated that ACT relieved OXA-induced decrease of platelet thrombocytopenia. Long-term administration of ACT markedly alleviates PLT aggregation in patients with cardiovascular risk factors (52). In addition, ACT improves immunity and protects liver function (53). Therefore, ACT may be a candidate for preventing thrombocytopenia and alleviating OXA-induced hematological toxicity. OXIN, a common adverse event in OXA chemotherapy, its incidence increases with dose (54), which limits the clinical use of oxaliplatin, sometimes leading to the end of treatment. ACT has been reported could attenuate hyperalgesia in the rat model with constriction and injury of the chronic sciatic nerve or sodium iodoacetate-induced inflammatory pain by intraperitoneal administration (55,56). The present study showed that ACT improved OXA-induced limb numbness and elevated the pain threshold in tumor-bearing nude mice. Therefore, the effects of ACT on OXIN may be associated with its neuroprotective activity. OXA could lead to aggravation of hepatic and renal injury, while the combination of ACT and OXA could attenuate hepatic and renal toxicity.

The transcriptomics and metabolomics analyses showed that ACT modulated the activity of signaling pathways, including 'phosphatidylinositol signaling system', 'inflammatory mediator regulation of TRP channels', 'inositol phosphate metabolism', 'amino sugar and nucleotide sugar metabolism' and 'aldosterone synthesis and secretion'. A total of eight genes/proteins, AKT1, PIK3R1, PLCB4, PRKCA, PTEN, INPP4B, INPP5D and PIKFYVE, were screened as the targets of ACT: PIK3R1 and PIKFYVE are polyphosphoinositides (PPIns) kinases, and PTEN, INPP4B and INPP5D are PPIns phosphatases. In the current study, OXA significantly reduced the levels of p-AKT1, AKT, p-PIK3R1 and PRKCA protein. However, the inhibitory effect observed was reversed when OXA was combined with ACT. This may be attributed to the role of the PI3K/AKT signaling pathway in mediating OXA-induced adverse effects. ACT mitigated these adverse effects by modulating this pathway, thereby alleviating OXA-induced toxicity.

Three genes, INPP4B, p53 and PTEN, have been reported to be essential for the PI3K/AKT signaling pathway (55). INPP4B has been reported to serve oncogenic and anti-oncogenic roles; however, to the best of our knowledge, it has rarely been reported in HCC prevention and treatment research (57,58). INPP4B, a member of the phosphatase family, primarily acts on the inositol ring of phosphatidylinositol 3,4-bisphosphate [PI(3,4)P2] to dephosphorylate PI(3,4)P2 to PI(3)P, and inhibits the phosphorylation of downstream AKT, thereby inhibiting PI3K/AKT signaling pathway and regulating tumor cell proliferation, metastasis and apoptosis (59,60). It has been reported that INPP4B is associated with numerous types of malignancy, such as prostate, breast, pancreatic, gastric, colorectal, ovarian and lung cancer (2,60-63). Tang *et al* (64) found INPP4B is a tumor suppressing gene in human HCC, and its overexpression inhibits the proliferation, migration, invasion as well as epithelial-to-mesenchymal transition and chemoresistance of cancer cells. In the present study, the INPP4B protein expression in the OXA and/or ACT groups, especially in the OXA + ACT group, showed significant upregulation compared with in the model group. Therefore, inhibiting the phosphatidylinositol signaling system by upregulating the expression of INPP4B may underlie the anti-HCC effects of OXA + ACT.

The PI3K/AKT signaling pathway, a key component in the phosphatidylinositol signaling system, is abnormally regulated in numerous types of malignant disease, such as HCC and gastric and breast cancer (65). It has been reported that the activated PI3K/AKT signaling pathway is necessary for HCC cell proliferation (66). ACT has been reported to reduce the expression of PI3K protein in tumor tissues (67). Attia *et al* (68) reported that ACT, as an adjuvant therapy, may synergize with 5-fluorouracil to treat colorectal cancer by inhibiting the PI3K/AKT signaling pathway. Consistently, OXA and/or ACT inhibited the PI3K/AKT signaling pathway in the present study. Furthermore, the tumor inhibitory effect of ACT + 2-morpholin-8-phenylchromone (Ly294002, a synthetic PI3K/AKT signaling pathway inhibitor) has been investigated in HepG2 xenograft nude mice: ACT, as a natural PI3K inhibitor exhibiting anti-HCC activity, exhibits a synergistic inhibitory effect on the growth of HepG2 xenografts in nude mice when combined with Ly294002 (69). These findings collectively suggested that the PI3K/AKT signaling pathway may be an important mechanism underlying the synergy OXA + ACT against HCC.

Upregulation of PI3K regulates the expression of tight junction proteins and impairs intestinal barrier function (59,70).

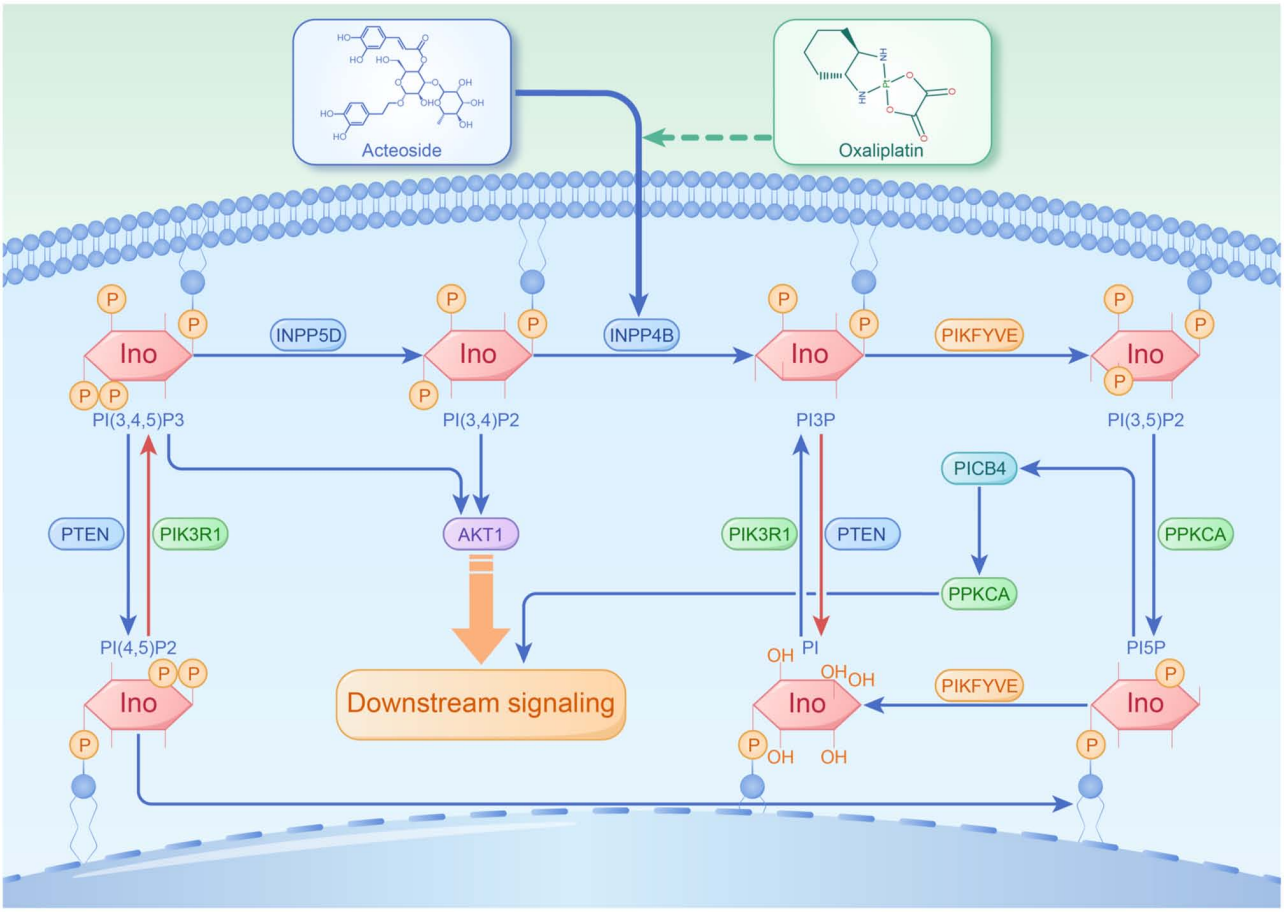

Figure 10. Putative mechanism of synergistic and toxicity-reducing effects of acteoside + oxaliplatin for treating hepatocellular carcinoma.

The PI3K/AKT signaling pathway also mediates PLT apoptosis via the mitochondrial pathway, which serves an important role in immune-mediated bone marrow failure thrombocytopenia (71). The PI3K-mediated signaling pathway could promote the adhesion and aggregation of PLTs (72), which suggests that PI3K may be a key target for the treatment of thrombocytopenia. In the present study, OXA + ACT attenuated thrombocytopenia and downregulated PI3K signaling, which indicated that ACT could alleviate OXA-induced thrombocytopenia by inhibiting the PI3K-mediated signaling pathway. Additionally, the PI3K/AKT signaling pathway is involved in the inflammatory response of acute liver injury, and its inhibition may regulate the inflammatory response and protect the liver (73). Moreover, the inhibition of the PI3K/AKT signaling pathway protects kidney cells due to its promoting effects on cisplatin-induced nephrotoxicity (74,75). The PI3K/AKT signaling pathway is also associated with activity of peripheral sympathetic nerves, and its abnormal activation leads to neuroinflammation and sympathetic hyperfunction. Conversely, its inhibition alleviates nerve injury (76). In addition, numerous studies have confirmed that voltage-gated sodium channels (VGSCs) are key targets of OXIN (47,77) and could be activated by phosphatidylinositol signaling (78). Therefore, ACT may inhibit VGSCs by deactivating the phosphatidylinositol signaling pathway, thereby alleviating OXIN. These data, together with the upregulated INPP4B expression in the present study, suggest that ACT may inhibit the PI3K/AKT signaling pathway by upregulating INPP4B, thereby alleviating OXA-induced side effects. Investigating the underlying mechanisms of ACT-alleviated OXIN may demonstrate the toxicity-reducing and synergistic effect of ACT as an adjuvant therapy of OXA in antagonizing HCC.

The present study has limitations. Firstly, although ACT is safe, the efficacy is not proportional to its dose. Excessive doses increase the metabolic burden of the liver and kidneys. The present study lacked pharmacokinetic data to explore the interaction between ACT and OXA. Therefore, the optimal administration ratio of ACT and OXA needs to be verified clinically. Secondly, given the synergism of ACT and OXA, cytochrome P450 enzymes should be studied in the future to understand ACT-OXA interactions. In addition, the inclusion of additional cell lines would strengthen the present findings by providing more comprehensive evidence of the synergistic effects of ACT and OXA. Contamination issues with commonly used cell lines, including human hepatocarcinoma cells SMCC-7721, rendered them unavailable. Future studies should use other cell lines to verify the synergistic effect of ACT and OXA. Additionally, the present study lacked positive controls (such as sorafenib) and functional validation. These analyses should be included in future studies to enhance the robustness of the present findings and confirm the efficacy of OXA + ACT. Furthermore, while the present study primarily focused on the synergistic effect of OXA + ACT, there may be off-target effects, potential drug interactions and toxicity concerns that

could contribute to the overall therapeutic outcome. Future studies should characterize the broader molecular interactions and unintended consequences associated with OXA + ACT. This will ensure a more comprehensive understanding of the safety and efficacy of this combination therapy.

In conclusion, ACT + OXA synergistically inhibited HCC cell proliferation, invasion and migration. In addition, ACT alleviated the toxicities induced by OXA, which was related to the regulation of multiple target genes/proteins including INPP4B, thereby inhibiting the PI3K/AKT signaling pathway (Fig. 10). The present findings may be useful for the clinical application of ACT and treatment strategies for HCC.

Acknowledgements

Not applicable.

Funding

The present study was supported by National Natural Science Foundation of China (grant no. 82360795), the Natural Science Foundation of Xinjiang Uygur Autonomous Region (grant no. 2021D01C347), the State Key Laboratory of Neurology and Oncology Drug Development Fund (grant no. SKLSIM-F-2024206) and the Public Hospital High Quality Development Scientific Research Public Welfare Project Fund (grant no. GL-A005).

Availability of data and materials

The data generated in the present study may be found in the Sequence Read Archive database under accession number PRJNA1219772) or at the following URL: https://www.ncbi.nlm.nih.gov/sra/PRJNA1219772.

Authors' contributions

LW designed the methodology, acquired funding, analyzed the data and wrote the original draft. JZ, BJ and ZR performed the experiments. HZ and YL participated in data analysis. LC and QH were involved in the amendment of the manuscript. JH and JY provided funding support and participated in designed the methodology. All authors read and approved the final version of the manuscript. LW and JY confirm the authenticity of all the raw data.

Ethics approval and consent to participate

All animal experiments were approved (approval no. IACUC-20210301-179) by the Experimental Animal Ethics Committee of First Affiliated Hospital of Xinjiang Medical University (Xinjiang, China).

Patient consent for publication

Not applicable.

Competing interests

The authors declare that they have no competing interests.

References

1. Wen N, Cai Y, Li F, Ye H, Tang W, Song P and Cheng N: The clinical management of hepatocellular carcinoma worldwide: A concise review and comparison of current guidelines: 2022 update. Biosci Trends 16: 20-30, 2022.
2. Guo ST, Chi MN, Yang RH, Guo XY, Zan LK, Wang CY, Xi YF, Jin L, Croft A, Tseng HY, *et al*: INPP4B is an oncogenic regulator in human colon cancer. Oncogene 35: 3049-3061, 2016.
3. Coriat R, Mir O, Cessot A, Brezault C, Ropert S, Durand JP, Cacheux W, Chaussade S and Goldwasser F: Feasibility of oxaliplatin, 5-fluorouracil and leucovorin (FOLFOX-4) in cirrhotic or liver transplant patients: Experience in a cohort of advanced hepatocellular carcinoma patients. Invest New Drugs 30: 376-381, 2012.
4. Petrelli F, Coinu A, Borgonovo K, Cabiddu M, Ghilardi M, Lonati V and Barni S: Oxaliplatin-based chemotherapy: A new option in advanced hepatocellular carcinoma. a systematic review and pooled analysis. Clin Oncol (R Coll Radiol) 26: 488-496, 2014.
5. Massarweh NN and El-Serag HB: Epidemiology of hepatocellular carcinoma and intrahepatic cholangiocarcinoma. Cancer Control 24: 1073274817729245, 2017.
6. Zhong Q, Li M and Shangguan X: Retrospective analysis of oxaliplatin adverse reactions/events based on database. Med Herald 39: 239-243, 2020 (In Chinese).
7. Wang H, Xu L and Zhao L: Literature analysis of 126 cases of oxaliplatin adverse reactions. Pharmacovigilance China 16: 110-114, 2019 (In Chinese).
8. Yu W, Zhang X and Huang Q: Protective Effect and Mechanism of Resveratrol on Peripheral Nerve Toxicity Induced by Oxaliplatin in Rats. Trad Chin Drug Res Clin Pharm 30: 20-25, 2019 (In Chinese).
9. Liu XW, Lou YN and Feng Z: Research status on efficacy enhancement and toxicity reduction of Chinese medicine in treatment of malignant tumors:a review of projects supported by National Natural Science Foundation of China. China J Chinese Materia Medica 47: 253-258, 2022 (In Chinese).
10. Wei Q, Li P, Yang T, Zhu J, Sun L, Zhang Z, Wang L, Tian X, Chen J, Hu C, *et al*: The promise and challenges of combination therapies with antibody-drug conjugates in solid tumors. J Hematol Oncol 17: 1, 2024.
11. Feng Y, An Q, Zhao Z, Wu M, Yang C, Liang W, Xu X, Jiang T and Zhang G: Beta-elemene: A phytochemical with promise as a drug candidate for tumor therapy and adjuvant tumor therapy. Biomed Pharmacother 172: 116266, 2024.
12. Liu H, Deng R, Zhu CW, Han HK, Zong GF, Ren L, Cheng P, Wei ZH, Zhao Y, Yu SY and Lu Y: Rosmarinic acid in combination with ginsenoside Rg1 suppresses colon cancer metastasis via co-inhition of COX-2 and PD1/PD-L1 signaling axis. Acta Pharmacol Sin 45: 193-208, 2024.
13. Gou B, Chen G, Huang S, Ning N, Gu Q, Duan S, Du Y, Nan Y and Yuan L: Review: Performance of jujube and its extracts in cancer: Therapeutic, toxicity-reducing and potentiating effects. Front Oncol 15: 1489974, 2025.
14. Li J, Fan S, Li H, Hu ZP and Hu Q: Evaluation of efficacy, safety and underlying mechanism on Traditional Chinese medicine as synergistic agents for cancer immunotherapy: A preclinical systematic review and meta-analysis. J Ethnopharmacol 338 (Pt 1): 119035, 2025.
15. Gao Q, Sheng Q, Yang Z, Zhu Z, Li L, Xu L, Xia J, Qiao Y, Gu J, Zhu X, *et al*: Honokiol-Magnolol-Baicalin Possesses synergistic anticancer potential and enhances the efficacy of Anti-PD-1 immunotherapy in colorectal cancer by triggering GSDME-dependent pyroptosis. Adv Sci (Weinh) 12: e2417022, 2025.
16. Sidhu H and Capalash N: Synergistic anti-cancer action of salicylic acid and cisplatin on HeLa cells elucidated by network pharmacology and in vitro analysis. Life Sci 282: 119802, 2021.
17. Chen L: Efficacy and mechanism of sorafenib combined with coix seed oil in the treatment of hepatocellular carcinoma. Lanzhou University, Lanzhou, 2018.
18. Sui J, Li F and Guo Y: Research progress on chemical constituents and pharmacological effects of Herba Cistanches and its predictive analysis of quality markers. J Liaoning Univ Trad Chin Med 23: 191-196, 2021 (In Chinese).
19. You S, Zhao J and Ma L: The effect and mechanism of ethanol extract of Herba Cistanches on immune hepatic fibrosis in rats. Chin J Pharm Toxicol 30: 504-510, 2016 (In Chinese).

20. Zhang A, Yang X, Li Q, Yang Y, Zhao G, Wang B and Wu D: Immunostimulatory activity of water-extractable polysaccharides from Cistanche deserticola as a plant adjuvant in vitro and in vivo. PLoS One 13: e0191356, 2018.
21. Guo Y, Meng S and Li Y: The effects of tonifying kidney and activating blood method adjuvant oxaliplatin in the treatment of gastrointestinal tumors. Med J Chin People Armed Police Forces 31: 707-710, 2020 (In Chinese).
22. Wen L, Hu J, Zhang J and Yang J: Phenylethanol glycosides from Herba Cistanche improve the hypoxic tumor microenvironment and enhance the effects of oxaliplatin via the HIF-1α signaling pathway. Mol Med Rep 24: 517, 2021.
23. Hei B, Wang J, Wu G, Ouyang J and Liu RE: Verbascoside suppresses the migration and invasion of human glioblastoma cells via targeting c-Met-mediated epithelial-mesenchymal transition. Biochem Biophys Res Commun 514: 1270-1277, 2019.
24. Jia WQ, Zhu JW, Yang CY, Ma J, Pu TY, Han GQ, Zou MM and Xu RX: Verbascoside inhibits progression of glioblastoma cells by promoting Let-7g-5p and down-regulating HMGA2 via Wnt/beta-catenin signalling blockade. J Cell Mol Med 24: 2901-2916, 2020.
25. Wei M, Cao L and Hui L: Research progress on anti-tumor mechanism of verbascoside. Guiding J Trad Chin Med Pharm 26: 125-128, 2020 (In Chinese).
26. Khan RA, Hossain R, Roy P, Jain D, Mohammad Saikat AS, Roy Shuvo AP, Akram M, Elbossaty WF, Khan IN, Painuli S, *et al*: Anticancer effects of acteoside: Mechanistic insights and therapeutic status. Eur J Pharmacol 916: 174699, 2022.
27. Xiao Y, Ren Q and Wu L: The pharmacokinetic property and pharmacological activity of acteoside: A review. Biomed Pharmacother 153: 113296, 2022.
28. Peerzada KJ, Faridi AH, Sharma L, Bhardwaj SC, Satti NK, Shashi B and Tasduq SA: Acteoside-mediates chemoprevention of experimental liver carcinogenesis through STAT-3 regulated oxidative stress and apoptosis. Environ Toxicol 31: 782-798, 2016.
29. Zhu B: Experimental study on the effect of verbascoside on the proliferation and autophagy of hepatocellular carcinoma cells through JNK signaling pathway. Lanzhou University, Lanzhou, 2020.
30. Mou JF, Lin XZ, Su HL, Lu HL, Liu QB, Liang B, Chen X, Liang CQ and Zhou XL: Anti-hepatitis B virus activity and hepatoprotective effect of des(rhamnosyl) verbascoside from Lindernia ruellioides in vitro. Phytother Res 35: 4555-4566, 2021.
31. Lee KJ, Woo ER, Choi CY, Shin DW, Lee DG, You HJ and Jeong HG: Protective effect of acteoside on carbon tetrachloride-induced hepatotoxicity. Life Sci 74: 1051-1064, 2004.
32. Chou TC: Theoretical basis, experimental design, and computerized simulation of synergism and antagonism in drug combination studies. Pharmacol Rev 58: 621-681, 2006.
33. Qin Y, Liu HJ, Li M, Zhai DH, Tang YH, Yang L, Qiao KL, Yang JH, Zhong WL, Zhang Q, *et al*: Salidroside improves the hypoxic tumor microenvironment and reverses the drug resistance of platinum drugs via HIF-1alpha signaling pathway. EBioMedicine 38: 25-36, 2018.
34. Ge SX, Son EW and Yao R: iDEP: An integrated web application for differential expression and pathway analysis of RNA-Seq data. BMC bioinformatics 19: 534, 2018.
35. Moreno-Torres M, García-Llorens G, Moro E, Méndez R, Quintás G and Castell JV: Factors that influence the quality of metabolomics data in in vitro cell toxicity studies: A systematic survey. Sci Rep 11: 22119, 2021.
36. Li G, Zhao CY, Wu Q, Guan SY, Jin HW, Na XL and Zhang YB: Integrated metabolomics and transcriptomics reveal di(2-ethylhexyl) phthalate-induced mitochondrial dysfunction and glucose metabolism disorder through oxidative stress in rat liver. Ecotoxicol Environ Saf 228: 112988, 2021.
37. Luchtel RA, Bhagat T, Pradhan K, Jacobs WR Jr, Levine M, Verma A and Shenoy N: High-dose ascorbic acid synergizes with anti-PD1 in a lymphoma mouse model. Proc Natl Acad Sci USA 117: 1666-1677, 2020.
38. Yang H, Lee HJ, Lee YG, Kim JW and Kim YS: Integrity of the untorn articular-sided tendon in bursal-sided partial-thickness rotator cuff tear: A comparative study of apoptotic activity in torn and untorn layers. Am J Sports Med 46: 2478-2485, 2018.
39. Juríková M, Danihel Ľ, Polák Š and Varga I: Ki67, PCNA, and MCM proteins: Markers of proliferation in the diagnosis of breast cancer. Acta Histochem 118: 544-552, 2016.
40. Jia WQ, Wang ZT, Zou MM, Lin JH, Li YH, Zhang L and Xu RX: Verbascoside inhibits glioblastoma cell proliferation, migration and invasion while promoting apoptosis through upregulation of protein tyrosine phosphatase SHP-1 and inhibition of STAT3 phosphorylation. Cell Physiol Biochem 47: 1871-1882, 2018.
41. Zhang Y, Yuan Y, Wu H, Xie Z, Wu Y, Song X, Wang J, Shu W, Xu J, Liu B, *et al*: Effect of verbascoside on apoptosis and metastasis in human oral squamous cell carcinoma. Int J Cancer 143: 980-991, 2018.
42. Chen WS: The diagnostic values of Ki-67 and Ezrin protein in the pathology of primary liver cancer. Jilin Med J 2: 2020 (In Chinese).
43. Pan LC, Xiao HY, Yin WJ and Lin Z: Correlation between HSD17B4 expression in rat liver cancer tissues and inflammation or proliferation. Eur Rev Med Pharmacol Sci 22: 3386-3393, 2018.
44. Wu WY, Yang Z and Long FX: Effects of Gehua Jieyu Recipe on GST-Pi and PCNA expressions and Wnt/β-catenin signaling pathway in precancerous lesions of ethanol-induced HBV transgenic mice. Chin J Immunol 36: 36-41, 2020 (In Chinese).
45. Ye Z, Gao X, Zhao B, Li H, Wan M, Wu N, Chang M and Cheng S: Diwu Yanggan capsule inhibits the occurrence and development of liver cancer in the Solt-Farber rat model by regulating the Ras/Raf/Mek/Erk signaling pathway. Am J Transl Res 10: 3797-3805, 2018.
46. Zhang JJ, Wang XP and Yang XY: Promoting effects of BANCR on the proliferation, invasion and angiogenesis of HepG2 hepatocellular carcinoma cells Chin J Immunol 34: 25-30, 2018 (In Chinese).
47. Kang L, Tian Y, Xu S and Chen H: Oxaliplatin-induced peripheral neuropathy: Clinical features, mechanisms, prevention and treatment. J Neurol 268: 3269-3282, 2021.
48. Hashemzadeh A, Amerizadeh F, Asgharzadeh F, Darroudi M, Avan A, Hassanian SM, Landarani M and Khazaei M: Delivery of oxaliplatin to colorectal cancer cells by folate-targeted UiO-66-NH(2). Toxicol Appl Pharmacol 423: 115573, 2021.
49. Oun R, Moussa YE and Wheate NJ: The side effects of platinum-based chemotherapy drugs: A review for chemists. Dalton Trans 47: 6645-6653, 2018.
50. Kobuchi S, Katsuyama Y and Ito Y: Mechanism-based pharmacokinetic-pharmacodynamic (PK-PD) modeling and simulation of oxaliplatin for hematological toxicity in rats. Xenobiotica 50: 223-230, 2020.
51. Lees JG, White D, Keating BA, Barkl-Luke ME, Makker PGS, Goldstein D and Moalem-Taylor G: Oxaliplatin-induced haematological toxicity and splenomegaly in mice. PLoS One 15: e0238164, 2020.
52. Campo G, Pavasini R, Biscaglia S, Ferri A, Andrenacci E, Tebaldi M and Ferrari R: Platelet aggregation values in patients with cardiovascular risk factors are reduced by verbascoside treatment. A randomized study. Pharmacol Res 97: 1-6, 2015.
53. Wu M, Yu S, Chen Y, Meng W, Chen H, He J, Shen J and Lin X: Acteoside promotes B cell-derived IL-10 production and ameliorates autoimmunity. J Leukoc Biol 112: 875-885, 2022.
54. Falcone A, Ricci S, Brunetti I, Pfanner E, Allegrini G, Barbara C, Crinò L, Benedetti G, Evangelista W, Fanchini L, *et al*: Gruppo oncologico nord ovest: Phase III trial of infusional fluorouracil, leucovorin, oxaliplatin, and irinotecan (FOLFOXIRI) compared with infusional fluorouracil, leucovorin, and irinotecan (FOLFIRI) as first-line treatment for metastatic colorectal cancer: The Gruppo Oncologico Nord Ovest. J Clin Oncol 25: 1670-1676, 2007.
55. Amin B, Poureshagh E and Hosseinzadeh H: The effect of verbascoside in neuropathic pain induced by chronic constriction injury in rats. Phytother Res 30: 128-135, 2016.
56. Wang WG, Wang P and Yang ZQ: Pharmacological effects of verbascoside: Research advances. J Intern Pharm Res 47: 1078-1087, 2020 (In Chinese).
57. Chen M, Nowak DG and Trotman LC: Molecular pathways: PI3K pathway phosphatases as biomarkers for cancer prognosis and therapy. Clin Cancer Res 20: 3057-3063, 2014.
58. Yuen JW, Chung GT, Lun SW, Cheung CC, To KF and Lo KW: Epigenetic inactivation of inositol polyphosphate 4-phosphatase B (INPP4B), a regulator of PI3K/AKT signaling pathway in EBV-associated nasopharyngeal carcinoma. PLoS One 9: e105163, 2014.
59. Chen T, Xue H, Lin R and Huang Z: MiR-126 impairs the intestinal barrier function via inhibiting S1PR2 mediated activation of PI3K/AKT signaling pathway. Biochem Biophys Res Commun 494: 427-432, 2017.

60. Zhuang B, Zhang J and Sun TQ, *et al*: Aflibercept alleviates high glucose-induced retinal pigment epithelial cell injury and PI3K/AKT signaling pathway activation. Chin J Histochem Cytochem 30: 235-239, 2021 (In Chinese).
61. Ren BY: Correlation of INPP4B gene on proliferation, metastasis and apoptosis of ovarian cancer cells. Dalian Medical University, 2018.
62. Yao JG: Expression and significance of SOX2 and CyclinD1 in epithelial ovarian carcinoma. Zhengzhou University, 2014.
63. Zhang L, Zeng D, Chen Y, Li N, Lv Y, Li Y, Xu X and Xu G: miR-937 contributes to the lung cancer cell proliferation by targeting INPP4B. Life Sci 155: 110-115, 2016.
64. Tang W, Yang L, Yang T, Liu M, Zhou Y, Lin J, Wang K and Ding C: INPP4B inhibits cell proliferation, invasion and chemoresistance in human hepatocellular carcinoma. Onco Targets Ther 12: 3491-3507, 2019.
65. Tang QF, Sun J and Yu H: Research progress on antitumor multidrug resistance of traditional Chin medicine based on PI3K/AKT signaling pathway. J Shanghai Univ Trad Chin Med 30: 78-82, 2016 (In Chinese).
66. Bamodu OA, Chang HL, Ong JR, Lee WH, Yeh CT and Tsai JT: Elevated PDK1 expression drives PI3K/AKT/MTOR signaling promotes radiation-resistant and dedifferentiated phenotype of hepatocellular carcinoma. Cells 9: 746, 2020.
67. Yang L, Zhang B, Liu J, Dong Y, Li Y, Li N, Zhao X, Snooks H, Hu C and Ma X: Protective effect of acteoside on ovariectomy-induced bone loss in mice. Int J Mol Sci 20: 2974, 2019.
68. Attia YM, El-Kersh DM, Wagdy HA and Elmazar MM: Verbascoside: Identification, quantification, and potential sensitization of colorectal cancer cells to 5-FU by targeting PI3K/AKT pathway. Sci Rep 8: 16939, 2018.
69. Wen LM, Zhang JW and Chen Z: Study on synergistic effect of acteoside combined with Ly294002 on transplanted human hepatocellular carcinoma in nude mice. Chin J Cancer Prev Treat 30: 904-911, 2023 (In Chinese).
70. Xing HZ, Sang F and Duan XY: Study on protective effect and mechanism of gallotannin on IFN-γ-induced Caco-2 cell monolayer barrier damage. J Chin Med Mater 44: 2663-2668, 2021 (In Chinese).
71. Xia LM, Yu H and Jin Z: Mechanism of PI3K/AKT mediated platelet apoptosis via mitochondrial pathway in thrombocytopenia in immune bone marrow failure. J Henan Univ (Med Sci) 41: 263-267+271, 2022 (In Chinese).
72. Chen X: The role and molecular mechanism of PI3K/Akt signaling pathway in megakaryocyte/platelet-mediated pathological process. Shanghai Jiaotong University, 2014.
73. Niu YB, Wang XL and Chen C: Effect of inhibition of PI3K-AKT-mTOR signaling pathway by metformin on acute liver injury induced by carbon tetrachloride in mice. Chin J Biol 34: 1062-1068+1075, 2021 (In Chinese).
74. Leng J: The protective effects of saponins from platycodi radix on cisplatin-induced nephrotoxicity via NF-κB and PI3K/AKT signaling pathway. Jilin Agricultural University, 2019.
75. Jiang S, Yang SQ and Zhou B: Lycopene protects kidney against nonylphenol-induced nephrotoxicity by regulating PI3K/Akt/p53 pathway. Chin J Vet Sci 42: 973-980, 2022 (In Chinese).
76. Zhang DD, Gu QY and You QX: Effects of hydrogen sulfide in paraventricular nuclei on blood pressure, peripheral sympathetic nerve activity and PI3K/Akt pathway in high salt-induced hypertensive rats. Chin J Tissue Engineer Res 27: 1-7, 2023 (In Chinese).
77. Xu LJ, Wang J, Li YD, Shen KF, He XH, Wu W and Liu CC: Reduction of SIRT1-mediated epigenetic upregulation of Nav1.7 contributes to oxaliplatin-induced neuropathic pain. Pain Physician 26: E213-E222, 2023.
78. Ma J, Long LH, Hu ZL, Zhang H, Han J, Ni L, Wang F, Chen JG and Wu PF: Activation of D1-like receptor-dependent phosphatidylinositol signal pathway by SKF83959 inhibits voltage-gated sodium channels in cultured striatal neurons. Brain Res 1615: 71-79, 2015.